Estimating winter balance and its uncertainty from direct measurements of snow depth and density on alpine glaciers

Alexandra PULWICKI,[1] Gwenn E. FLOWERS,[1] Valentina RADIĆ,[2] Derek BINGHAM[3]

[1] *Department of Earth Sciences, Faculty of Science, Simon Fraser University, Burnaby, BC, Canada*

[2] *Department of Earth, Ocean and Atmospheric Sciences, Faculty of Science, University of British Columbia, Vancouver, BC, Canada*

[3] *Department of Statistics and Actuarial Science, Faculty of Science, Simon Fraser University, Burnaby, BC, Canada*

Correspondence: Alexandra Pulwicki <apulwick@sfu.ca>

ABSTRACT. Accurately estimating winter surface mass balance on glaciers is central to assessing glacier health and predicting glacier runoff. However, measuring and modelling snow distribution is inherently difficult in mountainous terrain. Here we explore rigorous statistical methods of estimating winter balance and its uncertainty from multiscale measurements of snow depth and density. In May 2016 we collected over 9000 manual measurements of snow depth across three glaciers in the St. Elias Mountains, Yukon, Canada. Linear regression, combined with cross correlation and Bayesian model averaging, as well as ordinary kriging are used to interpolate point-scale values to glacier-wide estimates of winter balance. Elevation and a wind-redistribution parameter exhibit the highest correlations with winter balance, but the relationship varies considerably between glaciers. A Monte Carlo analysis reveals that the interpolation itself introduces more uncertainty than the assignment of snow density or the representation of grid-scale variability. For our study glaciers, the winter balance uncertainty from all assessed sources

ranges from 0.03 m w.e. (8%) to 0.15 m w.e. (54%). Despite the challenges associated with estimating winter balance, our results are consistent with a regional-scale winter-balance gradient.

INTRODUCTION

Winter surface mass balance, or "winter balance", is the net accumulation and ablation of snow over the winter season (Cogley and others, 2011), which constitutes glacier mass input. Winter balance (B_w) is half of the seasonally resolved mass balance, initializes summer ablation conditions and must be estimated to simulate energy and mass exchange between the land and atmosphere (e.g. Hock, 2005; Réveillet and others, 2016). Effectively representing the spatial distribution of snow on glaciers is also central to monitoring surface runoff and its downstream effects (e.g. Clark and others, 2011).

Winter balance (WB) is notoriously difficult to estimate (e.g. Dadić and others, 2010; Cogley and others, 2011). Snow distribution in alpine regions is highly variable with short correlation length scales (e.g. Anderton and others, 2004; Egli and others, 2011; Grünewald and others, 2010; Helbig and van Herwijnen, 2017; López-Moreno and others, 2011, 2013; Machguth and others, 2006; Marshall and others, 2006) and is influenced by dynamic interactions between the atmosphere and complex topography, operating on multiple spatial and temporal scales (e.g. Barry, 1992; Liston and Elder, 2006; Clark and others, 2011) (e.g. Barry, 1992; Liston and Elder, 2006; Clark and others, 2011; Scipión and others, 2013). Simultaneously extensive, high resolution and accurate snow distribution measurements on glaciers are therefore difficult to obtain (e.g. Cogley and others, 2011; McGrath and others, 2015). Physically based models are acquire (e.g. Cogley and others, 2011; McGrath and others, 2015) and obtaining such measurements is further complicated by the inaccessibility of many glacierized regions during the winter. Use of physically based models to estimate winter balance is computationally intensive and require requires detailed meteorological data to drive them the models (Dadić and others, 2010). As a result, there is significant uncertainty in estimates of winter balance, thus limiting the ability of models to represent current and projected glacier conditions.

Studies that have focused on obtaining detailed estimates of WB B_w have used a wide range of observational techniques, including direct measurement of snow depth and density (e.g. Cullen and others, 2017), lidar or photogrammerty (e.g. Sold and others, 2013) and ground-penetrating radar (e.g. Machguth and others, 2006; Gusmeroli and others, 2014; McGrath and others, 2015). Spatial coverage of direct measurements

is generally limited and often comprises an elevation transect along the glacier centreline (e.g. Kaser and others, 2003). Measurements are ~~often~~ typically interpolated using linear regression on only a few topographic parameters (e.g. MacDougall and Flowers, 2011), with elevation being the most common. Other established techniques include hand contouring (e.g. Tangborn and others, 1975), kriging (e.g. Hock and Jensen, 1999) and attributing measured winter balance values to elevation bands (e.g. Thibert and others, 2008). Physical snow models have been used to estimate spatial patterns of winter balance (e.g. Mott and others, 2008; Schuler and others, 2008; Dadić and others, 2010) but availability of the required meteorological data generally prohibits their widespread application. Error analysis is rarely undertaken and few studies have thoroughly investigated uncertainty in spatially distributed estimates of winter balance (c.f. Schuler and others, 2008).

More sophisticated snow-survey designs and statistical models of snow distribution are widely used in the field of snow science. Surveys described in the snow science literature are generally spatially extensive and designed to measure snow depth and density throughout a basin, ensuring that all terrain types are sampled. A wide array of measurement interpolation methods are used, including linear (e.g. López-Moreno and others, 2010) and non-linear regressions (e.g. Molotch and others, 2005) that include numerous terrain parameters, as well as geospatial interpolation ~~(e.g. Erxleben and others, 2002)~~ (e.g. Erxleben and others, 2002; Cullen and others, 2017) including various forms of kriging. Different interpolation methods are also combined; for example, regression kriging (see Supplementary Material) adds kriged residuals to a field obtained with linear regression (e.g. Balk and Elder, 2000). Physical snow models such as SnowTran-3D (Liston and Sturm, 1998), Alpine3D (Lehning and others, 2006), and SnowDrift3D (Schneiderbauer and Prokop, 2011) are widely used, and errors in estimating snow distribution have been examined from theoretical (e.g. Trujillo and Lehning, 2015) and applied perspectives (e.g. Turcan and Loijens, 1975; Woo and Marsh, 1978; Deems and Painter, 2006).

The goals of this study are to (1) critically examine methods of converting direct snow depth and density measurements to distributed estimates of winter balance and (2) identify sources of uncertainty, evaluate their magnitude and assess their combined contribution to uncertainty in glacier-wide winter balance. We focus on commonly applied, low-complexity methods of measuring and estimating winter balance in the interest of making our results broadly applicable.

STUDY SITE

The St. Elias Mountains (Fig. 1a) rise sharply from the Pacific Ocean, creating a significant climatic gradient between coastal maritime conditions, generated by Aleutian–Gulf of Alaska low-pressure systems, and interior
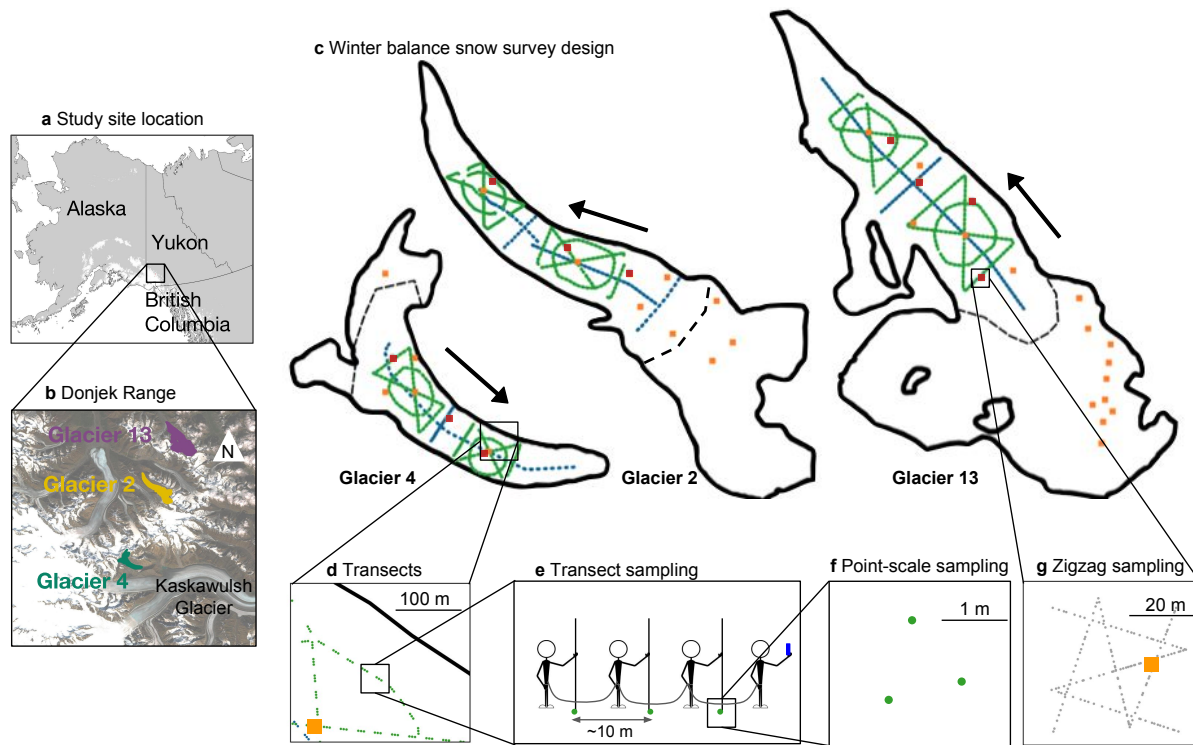
Fig. 1. Study area location and sampling design for Glaciers 4, 2 and 13. (a) Study region in the Donjek Range of the St. Elias Mountains of Yukon, Canada. (b) Study glaciers located along a southwest-northeast transect through the Donjek Range. The local topographic divide is shown as a dashed line. Imagery from Landsat8 (5 September 2013, data available from the U.S. Geological Survey). (c) Details of the snow-survey sampling design, with centreline and transverse transects (blue dots), hourglass and circle designs (green dots) and locations of snow density measurements (orange squares). Arrows indicate ice-flow directions. Approximate location of ELA on each glacier is shown as a black dashed line. (d) Close up of linear and curvilinear transects. (e) Configuration of navigator and observers. (f) Point-scale snow-depth sampling. (g) Linear-random snow-depth measurements in 'zigzag' design (~~grey~~ red dots) with one density measurement (orange square) per zigzag.

continental conditions, driven by the Yukon–Mackenzie high-pressure system (Taylor-Barge, 1969). The boundary between the two climatic zones is generally aligned with the divide between the Hubbard and Kaskawulsh Glaciers, approximately 130 km from the coast. Research on snow distribution and glacier mass balance in this area is limited. A series of research programs, including Project "Snow Cornice" and the Icefield Ranges Research Project, were operational in the 1950s and 60s (Wood, 1948; Danby and others, 2003) and in the last 30 years, there have been a few long-term studies on selected alpine glaciers (e.g. Clarke, 2014) as well as several regional studies of glacier mass balance and dynamics (e.g. Arendt and others, 2008; Burgess and others, 2013; Waechter and others, 2015).

Table 1. Physical characteristics of the study glaciers~~and May 2016 winter-balance survey details, including number of snow-depth measurement locations along transects (n_T), total length of transects (d_T), number of combined snow pit and Federal Sampler density measurement locations (n_ρ) and number of zigzag surveys (n_{zz}).~~

	~~Location~~ Location	Elevation (m a.s.l)			Slope (°)	Area
	~~UTM Zone 7~~ UTM Zone 7	*Mean*	*Range*	*ELA*	*Mean*	~~n_T d_T~~ **(km²)** ~~n_ρ n_{zz}~~
height**Glacier 4**	595470 E 6740730 N	2344	1958–2809	~2500	12.8	3.8 ~~4 7 May 2016 649 13.1 10 3~~
Glacier 2	601160 E 6753785 N	2495	1899–3103	~2500	13.0	7.0 ~~8 11 May 2016 762 13.6 11 3~~
Glacier 13	604602 E 6763400 N	2428	1923–3067	~2380	13.4	12.6

93   We carried out winter balance surveys on three unnamed glaciers in the Donjek Range of the St. Elias
94   Mountains. The Donjek Range is located approximately 40 km to the east of the regional mountain divide
95   and has an area of about $30 \times 30\,\text{km}^2$. Glacier 4, Glacier 2 and Glacier 13 (labelling adopted from Crompton
96   and Flowers (2016)) are located along a southwest-northeast transect through the range (Fig. 1b, Table 1).
97   These small alpine glaciers are generally oriented southeast-northwest, with Glacier 4 having a predominantly
98   southeast aspect and Glaciers 2 and 13 have generally northwest aspects. The glaciers are situated in valleys
99   with steep walls and have simple geometries. Based on a detailed study of Glacier 2 (Wilson and others,
100   2013) and related theoretical modelling (Wilson and Flowers, 2013) we suspect all of the study glaciers to
101   be polythermal.

Table 2. Details of the May 2016 winter-balance survey, including number of snow-depth measurement locations along transects (n_T), total length of transects (d_T), number of combined snow pit and Federal Sampler density measurement locations (n_ρ), number of zigzag surveys (n_{zz}), number (as percent of total number of gridcells, and of the number of gridcells in the ablation area) of gridcells sampled (n_S) and the elevation range (as percent of total elevations range and of ablation-area elevation range).

	Date	n_T	d_T **(km)**	n_ρ	n_{zz}	n_S	**Elevation range (m a.s.l.)**
Glacier 4	4–7 May 2016	649	13.1	7	3	295 (12%, 21%)	2015–2539 (62%, 97%)
Glacier 2	8–11 May 2016	762	13.6	7	3	353 (8%, 14%)	2151–2541 (32%, 47%)
Glacier 13	12–15 May 2016	941	18.1	~~20~~ 19	4	468 (6%, 14%)	2054–2574 (45%, 62%)

METHODS

Estimating glacier-wide winter balance (B_w) involves transforming measurements of snow depth and density into values of winter balance distributed across a defined grid (b_w). We do this in four steps. (1) Obtain direct measurements of snow depth and density in the field. (2) Assign density values to all depth-measurement locations to calculate point-scale values of b_w at each location. Winter balance, measured in units of metres water equivalent (m w.e.), can be estimated as the product of snow depth and depth-averaged density. (3) Average all point-scale values of b_w within each gridcell of a digital elevation model (DEM) to obtain the gridcell-averaged b_w. (4) Interpolate and extrapolate these gridcell-averaged b_w values to obtain estimates of b_w in each gridcell across the domain. B_w is then calculated by taking the average of all gridcell-averaged b_w values for each glacier. For brevity, we refer to these four steps as (1) field measurements, (2) density assignment, (3) gridcell-averaged b_w and (4) distributed b_w. Detailed methodology for each step is outlined below. We use the SPIRIT SPOT-5 DEM (40×40 m) from 2005 (Korona and others, 2009) throughout this study.

Field measurements

Our sampling campaign involved four people and occurred between 5–15 May 2016, which falls within the period of historical peak snow accumulation in southwestern Yukon (Yukon Snow Survey Bulletin and Water Supply Forecast, May 1, 2016). Snow depth is generally accepted to be more variable than density (Elder and others, 1991; Clark and others, 2011; López-Moreno and others, 2013) so we chose a sampling design that resulted in a high ratio ($\sim$55:1) of snow depth to density measurements. In total, we collected more than 9000 snow-depth measurements and more than 100 density measurements throughout the study area (Table).

During the field campaign there were two small accumulation events. The first, on 6 May 2016, also involved high winds so accumulation could not be determined. The second, on 10 May 2016, resulted in 0.01 m w.e accumulation measured at one location on Glacier 2. Assuming both accumulation events contributed a uniform 0.01 m w.e accumulation to all study glaciers then our survey did not capture $\sim$3% and $\sim$2% of estimated B_w on Glaciers 4 and 2, respectively. We therefore assume that these accumulation events were negligible and apply no correction. Positive temperatures and clear skies occurred between 11–16 May 2016, which we suspect resulted in melt occurring on Glacier 13. The snow in the lower part of the ablation area of Glacier 13 was isothermal and showed clear signs of melt and metamorphosis. The total amount of melt

131 during the study period was estimated using a degree-day model and found to be small (≤ 0.01 m w.e., see

132 Supplementary Material) so no corrections were made.

Sampling design

134 The snow surveys were designed to capture variability in snow depth at regional, basin, gridcell and point

135 scales (Clark and others, 2011). To capture variability at the regional scale we chose three glaciers along

136 a transect aligned with the dominant precipitation gradient (Fig. 1b) (Taylor-Barge, 1969). To account for

137 basin-scale variability, snow depth was measured along linear and curvilinear transects on each glacier (Fig.

138 1c) with a sample spacing of 10–60 m (Fig. 1d). Sample spacing was constrained by protocols for safe glacier

139 travel, while survey scope was constrained by the need to complete all surveys within the period of peak

140 accumulation. We selected centreline and transverse transects as the most commonly used survey designs

141 in winter balance studies (e.g. Kaser and others, 2003; Machguth and others, 2006) as well as an hourglass

142 pattern with an inscribed circle, which allows for sampling in multiple directions and easy travel (personal

143 communication from C. Parr, 2016). To capture variability at the grid scale, we densely sampled up to

144 four gridcells on each glacier using a linear-random sampling design (Shea and Jamieson, 2010) we term a

145 'zigzag'. To capture point-scale variability, each observer made 3–4 depth measurements within ~ 1 m (Fig.

146 1ef) at each transect measurement location. ~~In total, we collected more than 9000 snow-depth measurements~~

147 ~~throughout the study area (Table 1).~~

Snow depth: transects

149 ~~Winter balance can be estimated as the product of snow depth and depth-averaged~~

150 ~~density. Snow depth is generally accepted to be more variable than density~~

151 ~~(Elder and others, 1991; Clark and others, 2011; López-Moreno and others, 2013) so we chose a sampling~~

152 ~~design that resulted in a high ratio (~ 55:1) of snow depth to density measurements. Our sampling campaign~~

153 ~~involved four people and occurred between 5–15 May 2016, which falls within the period of historical peak~~

154 ~~snow accumulation in southwestern Yukon (Yukon Snow Survey Bulletin and Water Supply Forecast, May~~

155 ~~1, 2016).~~ While roped-up for glacier travel with fixed distances between observers, the lead observer used a

156 single-frequency GPS unit (Garmin GPSMAP 64s) to navigate between predefined transect measurement

157 locations (Fig. 1e). The remaining three observers used 3.2 m graduated aluminum avalanche probes to make

158 snow-depth measurements (Kinar and Pomeroy, 2015). The locations of each set of depth measurements,

159 made by the second, third and fourth observers, are estimated using the recorded location of the first

160 observer, the approximate distance between observers and the direction of travel. The 3–4 point-scale depth

161 measurements are averaged to obtain a single depth measurement at each transect measurement location.

162 When considering snow variability at the point scale as a source of uncertainty in snow depth measurements,

163 we find that the mean standard deviation of point-scale snow depth measurements is found to be <7% of

164 the mean snow depth for all study glaciers.

165 Snow-depth sampling was concentrated in the ablation area to ensure that only snow from the current

166 accumulation season was measured. The boundary between snow and firn in the accumulation area can be

167 difficult to detect and often misinterpreted, especially when using an avalanche probe (Grünewald and others,

168 2010; Sold and others, 2013). We intended to use a firn corer to measure winter balance in the accumulation

169 area, but cold snow combined with positive air temperatures led to cores being unrecoverable. Successful

170 snow depth ~~and density~~ measurements within the accumulation area were made either in snow pits or using

171 a Federal Sampler (described below) to unambiguously identify the snow–firn transition.

Snow depth: zigzags

173 ~~To capture snow-depth variability within a single DEM gridcell, we implemented a linear-random zigzag~~

174 ~~sampling design (Shea and Jamieson, 2010).~~ We measured depth at random intervals of 0.3–3.0 m along two

175 'Z'-shaped patterns (Shea and Jamieson, 2010), resulting in 135–191 measurements per zigzag, within three

176 to four ~~40 × 40~~ 40×40 m gridcells (Fig. 1g) per glacier. Random intervals were machine-generated from a

177 uniform distribution in sufficient numbers that each survey was unique. Zigzag locations were randomly

178 chosen within the upper, middle and lower regions of the ablation area of each glacier. ~~A fourth zigzag was~~

179 ~~measured~~ Extra time in the field allowed us to measure a fourth zigzag on Glacier 13 in the central ablation

180 area at ∼2200 m a.s.l.

Snow density

182 Snow density was measured using a Snowmetrics wedge cutter in three snow pits on each glacier~~, as~~

183 ~~well as with a Geo Scientific Ltd. metric Federal Sampler.~~ . Within the snow pits (SP), we measured

184 a vertical density profile (in ~~5~~ 10 cm increments) with the ~~5 × 10 × 10~~ $5 \times 5 \times 10$ cm wedge-shaped

185 cutter (250 cm^3) and a Presola 1000 g spring scale ~~(e.g. Gray and Male, 1981; Fierz and others, 2009)~~

186 (e.g. Gray and Male, 1981; Fierz and others, 2009; Kinar and Pomeroy, 2015). Wedge-cutter error is ap-

187 proximately ±6% (e.g. Proksch and others, 2016; Carroll, 1977). Uncertainty in estimating density from

188 ~~snow-pit~~ SP measurements also stems from incorrect assignment of density to layers that cannot be sampled

189 (e.g. ice lenses and hard layers). We attempt to quantify this uncertainty by varying estimated ice-layer

190 thickness by ±1 cm (≤100%) of the recorded thickness, ice layer density between 700 and 900 kg m^{-3} and

191 the density of layers identified as being too hard to sample (but not ice) between 600 and $700\,\text{kg}\,\text{m}^{-3}$.

192 When considering all three sources of uncertainty, the range of integrated density values is always less than

193 15% of the reference density. Depth-averaged densities for shallow pits ($<50\,\text{cm}$) that contain ice lenses are

194 particularly sensitive to changes in prescribed density and ice-lens thickness.

195 While ~~snow pits~~ SP provide the most accurate measure of snow density, digging and sampling a ~~snow~~

196 ~~pit~~ SP is time and labour intensive. Therefore, a ~~Federal Snow~~ Geo Scientific Ltd. metric Federal Sampler

197 (FS) (Clyde, 1932) with a 3.2–3.8 cm diameter sampling tube, which directly measures depth-integrated

198 snow-water equivalent, was used to augment the ~~snow pit~~ SP measurements. A minimum of three ~~Federal~~

199 ~~Sampler~~ FS measurements were taken at each of 7–19 locations on each glacier and an additional eight

200 ~~Federal Sampler~~ FS measurements were co-located with ~~each snow pit profile~~ two SP profiles for each glacier.

201 Measurements for which the snow core length inside the sampling tube was less than 90% of the snow depth

202 were discarded. Densities at each measurement location (eight at each ~~snow pit~~ SP, three elsewhere) were

203 then averaged, with the standard deviation taken to represent the uncertainty.

204 ~~During the field campaign there were two small accumulation events. The first, on 6 May 2016, also involved~~

205 ~~high winds so accumulation could not be determined. The second, on 10 May 2016, resulted in 0.01 m w.e~~

206 ~~accumulation measured at one location on Glacier 2. Positive temperatures and clear skies occurred between~~

207 ~~11–16 May 2016, which we suspect resulted in melt occurring on Glacier 13. The snow in the lower part of~~

208 ~~the ablation area of Glacier 13 was isothermal and showed clear signs of melt and metamorphosis. The total~~

209 ~~amount of accumulation and melt during the study period could not be estimated so no corrections were~~

210 ~~made~~ The mean standard deviation of FS-derived density was ≤4% of the mean density for all glaciers.

Density assignment

212 Measured snow density must be interpolated or extrapolated to estimate point-scale ~~winter balance~~ b_w at

213 each snow-depth sampling location. We employ four commonly used methods to interpolate and extrapolate

214 density (Table 3): (1) calculate mean density over an entire mountain range (e.g. Cullen and others, 2017),

215 (2) calculate mean density for each glacier (e.g. Elder and others, 1991; McGrath and others, 2015), (3)

216 linear regression of density on elevation for each glacier (e.g. Elder and others, 1998; Molotch and others,

217 2005) and (4) calculate mean density using inverse-distance weighting (e.g. Molotch and others, 2005) for

218 each glacier. Densities derived from ~~snow-pit (SP) measurements and the Federal Sampler (FS)~~ SP and

219 FS measurements are treated separately, for reasons explained below, resulting in eight possible methods of

220 assigning density.

Table 3. Eight methods used to estimate snow density at unmeasured locations. Total number of resulting density values given in parentheses, with n_T the total number of snow-depth measurement locations along transects (Table 1).

Method code	Source of measured snow density		Density assignment method
	Snow pit	*Federal Sampler*	
S1	■		Mean of measurements
F1		■	across all glaciers (1)
S2	■		Mean of measurements
F2		■	for each glacier (3)
S3	■		Regression of density on
F3		■	elevation for a glacier (n_T)
S4	■		Inverse distance weighted
F4		■	mean for a glacier (n_T)

Gridcell-averaged winter balance

We average one to six (mean of 2.1 measurements) point-scale values of ~~WB within each 40 × 40 m~~ b_w within each DEM gridcell to obtain the gricell-averaged ~~WB~~b_w. The locations of individual measurements have uncertainty due to the error in the horizontal position given by the GPS unit and the estimation of observer location based on the recorded GPS positions of the navigator. This location uncertainty could result in the incorrect assignment of a point-scale ~~WB~~ b_w measurement to a particular gridcell. However, this source of error is not further investigated because we assume that the uncertainty ~~in gridcell-averaged WB~~ resulting from incorrect locations of point-scale b_w values is captured in the ~~zigzag measurements~~ uncertainty derived from zigzag measurements, as described below. ~~Uncertainty~~ Error due to having multiple observers ~~was also evaluated . There are~~ is also evaluated by conducting an analysis of variance (ANOVA) of snow-depth measurement along a transect and testing for differences between observers. We find no significant differences between snow-depth measurements made by observers along any transect (p>0.05), with the exception of the first transect on Glacier 4 (51 measurements)~~.~~, where snow depth values collected by one observer were, on average, greater than the snow depth measurements taken by the other two observers (p<0.01). Since this was the first transect and the only one to show differences by observer, this difference can be considered

236 an anomaly. We conclude that observer bias is not an important effect in this study and therefore apply no

237 observer corrections to the data.

Distributed winter balance

239 Gridcell-averaged values of ~~WB~~ b_w are interpolated and extrapolated across each glacier using linear

240 regression (LR) and ~~simple kriging (SK~~ordinary kriging (OK). The ~~regression~~ LR relates gridcell-averaged

241 ~~WB and~~ b_w to various topographic parameters ~~, as this method~~ and we use this method because it is

242 simple and has precedent for success (e.g. McGrath and others, 2015). Instead of a basic ~~regression~~ LR

243 however, we use cross-validation ~~and~~ to prevent data overfitting as well as model averaging to ~~test~~ allow for

244 all combinations of the chosen topographic parameters. We compare the ~~regression approach with simple~~

245 ~~kriging (SK)~~LR approach with OK, a data-driven interpolation method free of any physical interpretation

246 (e.g. Hock and Jensen, 1999).

Linear regression

248 In the ~~regression~~LR, we use commonly applied topographic parameters as in McGrath and others (2015),

249 including elevation, slope, aspect, curvature, "northness" and a wind-redistribution parameter $(Sx$ from

250 Winstral and others (2002)); we add distance-from-centreline as an additional parameter. Topographic

251 parameters are standardized for use in the LR. For details on data and methods used to estimate the

252 topographic parameters see the Supplementary Material and Pulwicki (2017). Our sampling design ensured

253 that the ranges of topographic parameters associated with our measurement locations represent more than

254 70% of the total area of each glacier (except elevation on Glacier 2, where our measurements captured only

255 50%). ~~Topographic parameters are standardized and then weighted by~~

256 The goal of the LR is to obtain a set of fitted regression coefficients (β_i) ~~calculated by minimizing the sum~~

257 ~~of squares of the vertical deviations of each datum from the regression line (Davis and Sampson, 1986). For~~

258 ~~details on data and methods used to estimate the topographic parameters see the Supplementary Material.~~

259 ~~To~~ that correspond to each topographic parameter and to a model intercept. The LR implemented in this

260 study is an extension of a basic multiple linear regression; we use cross-validation to avoid overfitting the data

261 and model averaging to incorporate every possible combination of topographic parameters~~, cross-validation~~

262 ~~and model averaging are implemented.~~

263 First, cross-validation is used to obtain a set of β_i ~~values~~ that have the greatest predictive ability

264 (Kohavi and others, 1995). We randomly select 1000 subsets of the data (2/3 of the values) ~~to fit the LR~~

265 ~~and~~ and fit a basic multiple linear regression (implemented in MATLAB) to the data subsets, thus obtaining

266 1000 sets of β_i. The basic multiple linear regression calculates a set of β_i by minimizing the sum of squares

267 of the vertical deviations of each datum from the regression line (Davis and Sampson, 1986). Distributed b_w

268 is then calculated using each set of β_i by weighting topographic parameters by their corresponding β_i values

269 for all DEM gridcells. We then use the remaining data (1/3 of the values) to calculate a root mean squared

270 error (RMSE) ~~(Kohavi and others, 1995)~~between the estimated b_w and the observed b_w for corresponding

271 locations. From the 1000 sets of β_i values, we select the set that results in the lowest RMSE.

272   Second, we use model averaging to account for uncertainty when selecting predictors and to maximize the

273 model's predictive ability (Madigan and Raftery, 1994). Models are generated by calculating a set of β_i (as

274 described above) for all possible combinations of topographic parameters~~,~~, resulting in 2^7 models (i.e. 2^7

275 sets of β_i with the greatest predictive ability for each linear combination of topographic parameters). Using

276 a Bayesian framework, model averaging involves weighting all models by their posterior model probabilities

277 (Raftery and others, 1997). ~~To obtain the final regression coefficients, the β_i values from each model are~~

278 ~~weighted according to the~~ We weight the models according to their relative predictive success~~of the model~~,

279 as assessed by the value of the Bayesian Information Criterion (BIC) (Burnham and Anderson, 2004). BIC

280 penalizes more complex models, which further reduces the risk of overfitting. The ~~distributed WB is then~~

281 final set of β_i is then the weighted sum of β_i from all models. Distributed b_w is obtained by applying the

282 ~~resulting regression coefficients~~ final set of β_i to the topographic parameters associated with each gridcell.

283 *~~Simple~~ Ordinary kriging*

284 ~~Simple kriging (SK)~~ Kriging is a data-driven method of estimating variables at unsampled locations by

285 using the isotropic spatial correlation (covariance) of measured values to find a set of optimal weights

286 (Davis and Sampson, 1986; Li and Heap, 2008). ~~Simple kriging~~ Kriging assumes spatial correlation between

287 sampling locations that are distributed across a surface and then applies the correlation to interpolate

288 between these locations. Many forms of kriging have been developed to accommodate different data types

289 (e.g. Li and Heap, 2008, and sources within). Ordinary kriging (OK) is the most basic form of kriging where

290 the mean of the estimated field is unknown. Unlike LR, OK is not useful for generating hypotheses to explain

291 the physical controls on snow distribution, nor can it be used to estimate winter balance on unmeasured

292 glaciers. However, we chose to use OK because it does not require external inputs and is therefore a means

293 of obtaining B_w that is free of physical interpretation beyond the information contained in the covariance

294 matrix.

We used the `DiceKriging` R package (Roustant and others, 2012) to calculate the maximum likelihood covariance matrix, as well as the range distance (θ) and nugget for gridcell-averaged values of winter balance. The range distance is a measure of data correlation length and the nugget is the residual that encompasses sampling-error variance as well as the spatial variance at distances less than the minimum sample spacing (Li and Heap, 2008). ~~Unlike topographic regression, simple kriging is not useful for generating hypotheses to explain the physical controls on snow distribution, nor can it be used to estimate winter balance on unmeasured glaciers~~A Matére covariance function with $\nu=5/2$ is used to define a stationary and isotropic covariance and covariance kernels are parameterized as in Rasmussen and Williams (2006).

Uncertainty analysis using a Monte Carlo approach

Three sources of uncertainty are considered separately: the uncertainty due to (1) grid-scale variability of b_w (σ_GS), (2) the assignment of snow density (σ_ρ) and (3) interpolating and extrapolating gridcell-averaged values of b_w (σ_INT). To quantify the uncertainty of grid-scale and interpolation uncertainty on estimates of ~~glacier-wide WB~~ B_w we conduct a Monte Carlo analysis, which uses repeated random sampling of input variables to calculate a distribution of output variables (Metropolis and Ulam, 1949). We repeat the random sampling process 1000 times, resulting in a distribution of values of the ~~glacier-wide WB~~ B_w based on uncertainties associated with the four steps outlined above. ~~We use the standard deviation of this distribution as a useful metric of uncertainty on the glacier-wide WB. Three~~ Individual sources of uncertainty are ~~considered separately: the uncertainty due to (1) grid-scale variability of WB (σ_GS), (2) the assignment of snow density (σ_ρ) and (3) interpolating and extrapolating gridcell-averaged values of WB (σ_INT). These individual sources of uncertainty are~~ propagated through the conversion of snow depth and density measurements to ~~glacier-wide WB~~B_w. Finally, the combined effect of all three sources of uncertainty on the ~~glacier-wide WB~~ B_w is quantified. We use the standard deviation of the distribution of B_w as a useful metric of B_w uncertainty. Density assignment uncertainty is calculated as the standard deviation of the eight resulting values of B_w. We calculate a relative uncertainty, as the normalized sum of differences between every pair of one hundred distributed ~~WB~~ b_w estimates including σ_GS and σ_INT, to investigate the spatial patterns in b_w uncertainty.

Grid-scale uncertainty (σ_GS)

We make use of the zigzag surveys to quantify the true variability of ~~WB~~ b_w at the grid scale. Our limited data do not permit a spatially-resolved assessment of grid-scale uncertainty, so we characterize this uncertainty as uniform across each glacier and represent it by a normal distribution. The distribution is centred at zero and

has a standard deviation equal to the mean standard deviation of all zigzag measurements for each glacier. For each iteration of the Monte Carlo, ~~WB~~ b_{w} values are randomly chosen from the distribution and added to the values of gridcell-averaged ~~WB~~ b_{w}. These perturbed gridcell-averaged values of ~~WB~~ b_{w} are then used in the interpolation. We represent uncertainty in ~~glacier-wide WB~~ B_{w} due to grid-scale uncertainty (σ_{GS}) as the standard deviation of the resulting distribution of ~~glacier-wide WB~~ B_{w} estimates.

Density assignment uncertainty (σ_{ρ})

We incorporate uncertainty due to the method of density assignment by carrying forward all eight density interpolation methods (Table 3) when estimating ~~glacier-wide WB~~ B_{w}. By choosing to retain even the least plausible options, as well as the questionable FS data, this approach results in a generous assessment of uncertainty. We represent the ~~glacier-wide WB~~ B_{w} uncertainty due to density assignment uncertainty (σ_{ρ}) as the standard deviation of ~~glacier-wide WB~~ B_{w} estimates calculated using each density assignment method.

Interpolation uncertainty (σ_{INT})

We represent the uncertainty due to interpolation/extrapolation of gridcell-averaged ~~WB~~ b_{w} in different ways for LR and ~~SK~~ OK. LR interpolation uncertainty is represented by a multivariate normal distribution of possible regression coefficients (β_i). The standard deviation of each distribution is calculated using the covariance of ~~regression coefficients~~ β_i as outlined in Bagos and Adam (2015), which ensures that ~~regression coefficients~~ β_i are internally consistent. The β_i distributions are randomly sampled and used to calculate gridcell-estimated ~~WB~~ b_{w}.

~~SK~~ OK interpolation uncertainty is represented by the ~~95% confidence interval for~~ standard deviation for each gridcell-estimated ~~values of WB~~ value of b_{w} generated by the `DiceKriging` package. ~~From this confidence interval, the standard deviation of each gridcell-estimated WB is then calculated.~~ The standard deviation of ~~glacier-wide WB~~ B_{w} is then found by taking the square root of the average variance of each gridcell-estimated ~~WB~~ b_{w}. The final distribution of ~~glacier-wide WB~~ B_{w} values is centred at the ~~glacier-wide WB estimated with SK~~ B_{w} estimated with OK. For simplicity, the standard deviation of ~~glacier-wide WB~~ B_{w} values that result from either LR or ~~SK interpolation~~ OK interpolation/extrapolation uncertainty is referred to as σ_{INT}.
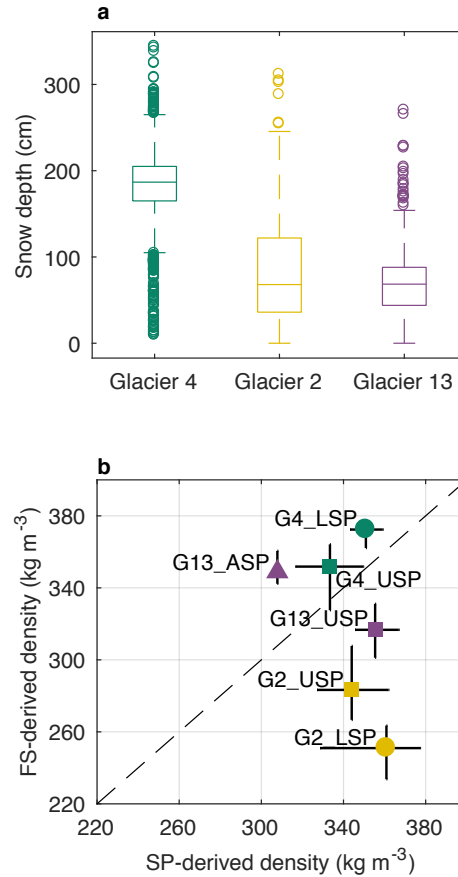
Fig. 2. Measured snow depth and density. (a) Boxplot of measured snow depth on Glaciers 4, 2 and 13 with the first quartiles (box), median (line within box), minimum and maximum values excluding outliers (bar) and outliers (circles), which are defined as being outside of the range of 1.5 times the quartiles (approximately $\pm 2.7\sigma$). (b) Comparison of depth-averaged densities estimated using Federal Sampler (FS) measurements and a wedge cutter in a snow pit (SP) for Glacier 4 (G4), Glacier 2 (G2) and Glacier 13 (G13). Labels indicate ~~snow pit~~ SP locations in the accumulation area (ASP), upper ablation area (USP) and lower ablation area (LSP). Error bars for SP-derived densities are calculated by varying the thickness and density of layers that are too hard to sample, and error bars for FS-derived densities are the standard deviation of measurements taken at one location. One-to-one line is dashed.

RESULTS~~AND DISCUSSION~~

Field measurements

Snow depth

Mean snow depth varied systematically across the study region, with Glacier 4 having the highest mean snow depth and Glacier 13 having the lowest (Fig. 2a). At each measurement location, the median range of measured depths (3–4 points) as a percent of the mean local depth is 2%, 11% and 12%, for Glaciers 4, 2 and 13, respectively. While Glacier 4 has the lowest point-scale variability, as assessed above, it also has
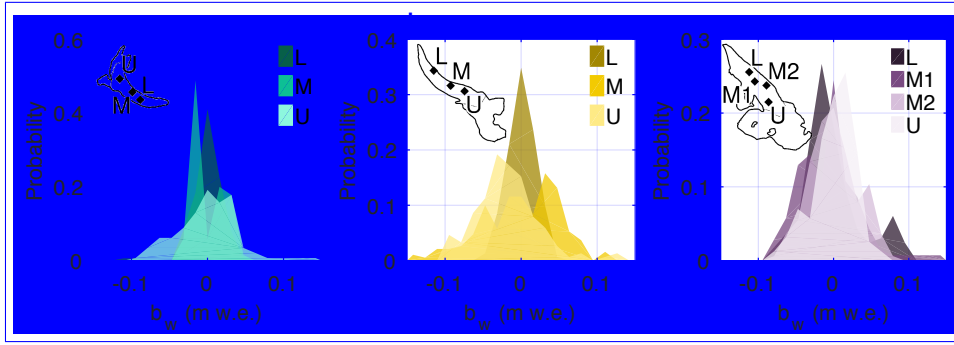
Fig. 3. Distributions of estimated winter-balance values for each zigzag survey in lower (L), middle (M) and upper (U) ablation areas (insets). Local mean has been subtracted. (a) Glacier 4. (b) Glacier 2. (c) Glacier 13.

the highest proportion of outliers, indicating a more variable snow depth across the glacier. The average standard deviation of all zigzag depth measurements is 0.07 m, 0.17 m and 0.14 m, for Glaciers 4, 2 and 13, respectively. When converted to values of ~~WB~~ b_w using the local FS-derived density measurement, the average standard deviation is 0.027 m w.e., 0.035 m w.e. and 0.040 m w.e. ~~WB~~ Winter-balance data for each zigzag are not normally distributed (Fig. 3).

Snow density

Contrary to expectation, co-located FS and SP measurements are found to be uncorrelated ($R^2 = 0.25$, Fig. 2b). The ~~Federal Sampler~~ FS appears to oversample in deep snow and undersample in shallow snow. Oversampling by small-diameter ~~(3.2–3.8 cm)~~ sampling tubes has been observed in previous studies, with a percent error between 6.8% and 11.8% (e.g. Work and others, 1965; Fames and others, 1982; Conger and McClung, 2009). Studies that use ~~Federal Samplers~~ FS often apply a 10% correction to all measurements for this reason (e.g. Molotch and others, 2005). Oversampling has been attributed to slots "shaving" snow into the tube as it is rotated (e.g. Dixon and Boon, 2012) and to snow falling into the slots, particularly for snow samples with densities $>400\,\mathrm{kg\,m^{-3}}$ and snow depths >1 m (e.g. Beaumont and Work, 1963). Undersampling is likely to occur due to loss of snow from the bottom of the sampler (Turcan and Loijens, 1975). Loss by this mechanism may have occurred in our study, given the isothermal and melt-affected snow conditions observed over the lower reaches of Glaciers 2 and 13. Relatively poor ~~Federal Sampler~~ FS spring-scale sensitivity also calls into question the reliability of measurements for snow depths <20 cm.

Our FS-derived density values are positively correlated with snow depth ($R^2 = 0.59$). This relationship could be a result of physical processes, such as compaction in deep snow and preferential formation of depth hoar in shallow snow, but is more likely a result of measurement artefacts for a number of reasons. First, the

379 total range of densities measured by the ~~Federal Sampler~~ FS seems improbably large $(227–431\,\mathrm{kg\,m^{-3}})$~~given~~

380 ~~the conditions at the~~ . At the time of sampling the snow pack had little new snow, which confounds the

381 low density values, and was not yet saturated and had few ice lenses, which confounds the high density

382 values. Moreover, the range of FS-derived values is much larger than ~~than~~ that of SP-derived values when

383 co-located measurements are compared. Second, compaction effects of the magnitude required to explain the

384 density differences between SP and FS measurements would not be expected at the measured snow depths

385 (up to $340\,\mathrm{cm}$). Third, no linear relationship exists between depth and SP-derived density ($R^2 = 0.05$). These

386 findings suggest that the ~~Federal Sampler~~ FS measurements have a bias for which we have not identified a

387 suitable correction. Despite this bias, we use FS-derived densities to generate a range of possible b_w estimates

388 and to provide a generous estimate of uncertainty arising from density assignment.

Density assignment

390 Given the lack of correlation between co-located SP- and FS-derived densities (Fig. 2), we use the densities

391 derived from these two methods separately (Table 3). SP-derived regional (S1) and glacier-mean (S2) densities

392 are within one standard deviation of the corresponding FS-derived densities (F1 and F2) although SP-derived

393 density values are larger (see Supplementary Material, Table ~~S2~~S3). For both SP- and FS-derived densities,

394 the mean density for any given glacier (S2 or F2) is within one standard deviation of the mean across all

395 glaciers (S1 or F1). Correlations between elevation and SP- and FS-derived densities are generally high

396 ($R^2 > 0.5$) but vary between glaciers (Supplementary material, Table ~~S2~~S3). For any given glacier, the

397 standard deviation of the 3–4 SP- or FS-derived densities is <13% of the mean of those values (S2 or F2)

398 (Supplementary material, Table ~~S2~~S3). We adopt S2 (glacier-wide mean of SP-derived densities) as the

399 reference method of density assignment. Though the method described by S2 does not account for known

400 basin-scale spatial variability in snow density (e.g. Wetlaufer and others, 2016), it is commonly used in winter

401 balance studies (e.g. Elder and others, 1991; McGrath and others, 2015; Cullen and others, 2017).

Gridcell-averaged winter balance

403 The distributions of gridcell-averaged ~~WB~~ b_w values for the individual glaciers are similar to those in Fig. 2a

404 but with fewer outliers ~~.~~ (see Supplementary Material, Fig. S4). The standard deviations of ~~WB~~ b_w values

405 determined from the zigzag surveys are almost twice as large as the mean standard deviation of point-scale

406 ~~WB~~ b_w values within a gridcell measured along transects ~~.~~ (see Supplementary Material, Fig. S5). However,

407 a small number of gridcells sampled in transect surveys have standard deviations in ~~WB~~ b_w that exceed

Table 4. Glacier-wide winter balance (~~WB~~B_w, m w.e.) estimated using linear regression and ~~simple~~ ordinary kriging for the three study glaciers. Root mean squared error (RMSE, m w.e.) is computed as the average of all RMSE values between gridcell-averaged values of ~~WB~~ b_w (the data) that were randomly selected and excluded from interpolation (1/3 of all data) and those estimated by interpolation. RMSE as a percent of the ~~glacier-wide WB~~ B_w is shown in brackets.

	Linear regression		Ordinary kriging	
	~~WB~~ B_w	RMSE	~~WB~~ B_w	RMSE
G4	0.58	0.15 (26%)	0.62	~~0.13 (21~~0.11 (18%)
G2	0.58	0.10 (17%)	~~0.37~~ 0.35	~~0.07 (19~~0.06 (18%)
G13	0.38	0.08 (21%)	0.27	~~0.07 (26~~0.06 (21%)

408 0.25 m w.e. (~10 times greater than those for zigzag surveys). ~~We nevertheless assume that the gridcell~~

409 ~~uncertainty is captured with dense sampling in zigzag gridcells.~~

410 ~~Distribution of coefficients (β_i) determined by linear regression of gridcell-averaged WB on DEM-derived~~

411 ~~topographic parameters for the eight different density assignment methods (Table 3). Coefficients are~~

412 ~~calculated using standardized data, so values can be compared across parameters. Regression coefficients~~

413 ~~that are not significant are assigned a value of zero. Topographic parameters include elevation (z), distance~~

414 ~~from centreline (d_C), slope (m), curvature (κ) and wind redistribution (Sx). Aspect (α) and "northness"~~

415 ~~(N) are not shown because coefficient values are zero in every case. The box plot shows first quartiles~~

416 ~~(box), median (line within box), mean (circle within box), minimum and maximum values excluding outliers~~

417 ~~(bars) and outliers (gray dots), which are defined as being outside of the range of 1.5 times the quartiles~~

418 ~~(approximately $\pm 2.7\sigma$).~~

419 ## Distributed winter balance

420 ## ~~Distributed winter balance~~

421 ~~Relative uncertainty in distributed winter balance (WB) (Fig. 4) found using linear regression (top row) and~~

422 ~~simple kriging (bottom row). Values closer to one indicate higher relative uncertainty. Ice-flow directions are~~

423 ~~indicated by arrows.~~

424 *Linear regression*

425 The highest values of estimated b_w are found in the upper portions of the accumulation areas of Glaciers

426 2 and 13 (Fig. 4). These areas also correspond to large values of elevation, slope, and wind redistribution.

427 Extrapolation of the positive relation between b_w and elevation, as well as slope and Sx for Glacier 2, results
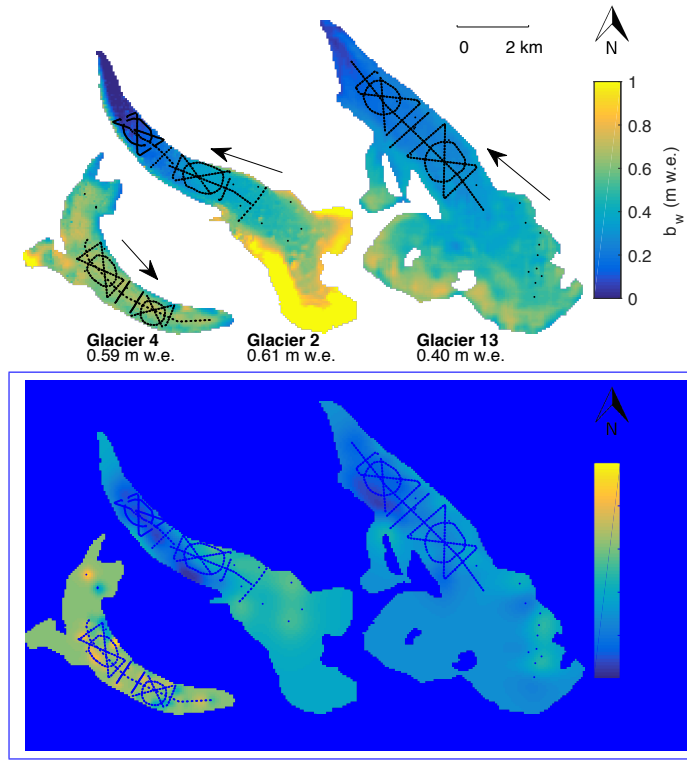
Fig. 4. Spatial distribution of winter balance (~~WB~~b_w) estimated using linear regression (top row) and ~~simple~~ ordinary kriging (bottom row) with densities assigned as per S2 (Table 3). The linear regression (LR) method involves multiplying regression coefficients, found using cross validation and model averaging, by topographic parameters for each gridcell. Ordinary kriging (OK) uses the covariance of measured values to find a set of optimal weights for estimating values at unmeasured locations. Locations of snow-depth measurements made in May 2016 are shown as black dots. Ice-flow directions are indicated by arrows. Values of ~~glacier-wide WB~~ B_w are given below labels.

428   in high b_w estimates and large relative uncertainty in these estimates (Fig. 5). On Glacier 4, the distributed

429   b_w and the relative uncertainty are almost uniform (Fig. 4) due to the small regression coefficients for

430   all topographic parameters. The explained variance of the LR-estimated b_w differs considerably between

431   glaciers (Fig. 6), with the best correlation between modelled- and observed-b_w occurring for Glacier 2. LR is

432   an especially poor predictor of b_w on Glacier 4, where B_w can be estimated equally well using the mean of

433   the data. RMSE is also highest for Glacier 4 (Table 4).

434   *Ordinary kriging*

435   For all three glaciers, large areas that correspond to locations far from measurements have b_w estimates

436   equal to the kriging mean. Distributed b_w estimated with OK on Glacier 4 is mostly uniform except for local

437   deviations close to measurement locations (Fig. 4) and relative uncertainty is highest close to measurement

438   locations. Distributed b_w varies more smoothly on Glaciers 2 and 13 (Fig. 4). Glacier 2 has a distinct region
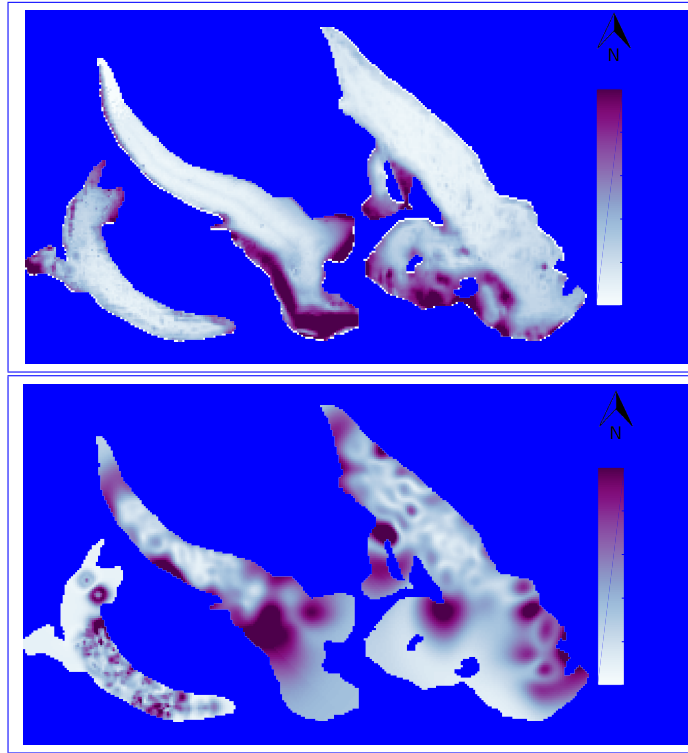
Fig. 5. Relative uncertainty in distributed winter balance (b_w) (Fig. 4) found using linear regression (top row) and ordinary kriging (bottom row). Values closer to one indicate higher relative uncertainty. Ice-flow directions are indicated by arrows.

439   of low estimated b_w (~0.1 m w.e.) in the lower part of the ablation area, which corresponds to a wind-scoured

440   region of the glacier. Glacier 13 has the lowest estimated mean b_w and only small deviations from this mean

441   at measurement locations (Fig. 4). Relative uncertainty vary considerably across the three study glaciers with

442   the greatest uncertainty just outside of the region with observed b_w (Fig. 5). As expected, explained variance

443   of OK-estimated b_w is high for both Glaciers 2 and 13 (Fig. 6) because OK is a data-fitting algorithm.

444   However, explained variance (Fig. 6) for Glacier 4 is relatively low and RMSE is relatively high (Table 4),

445   indicating a highly variable distribution of b_w.

446   ## Uncertainty analysis using a Monte Carlo approach

447   *Linear Regression*

448   Glacier-wide winter balance is affected by uncertainty introduced by the representativeness of

449   gridcell-averaged values of b_w (σ_{GS}), choosing a method of density assignment (σ_ρ), and

450   interpolating/extrapolating b_w values across the domain (σ_{INT}). Using a Monte Carlo analysis, we find

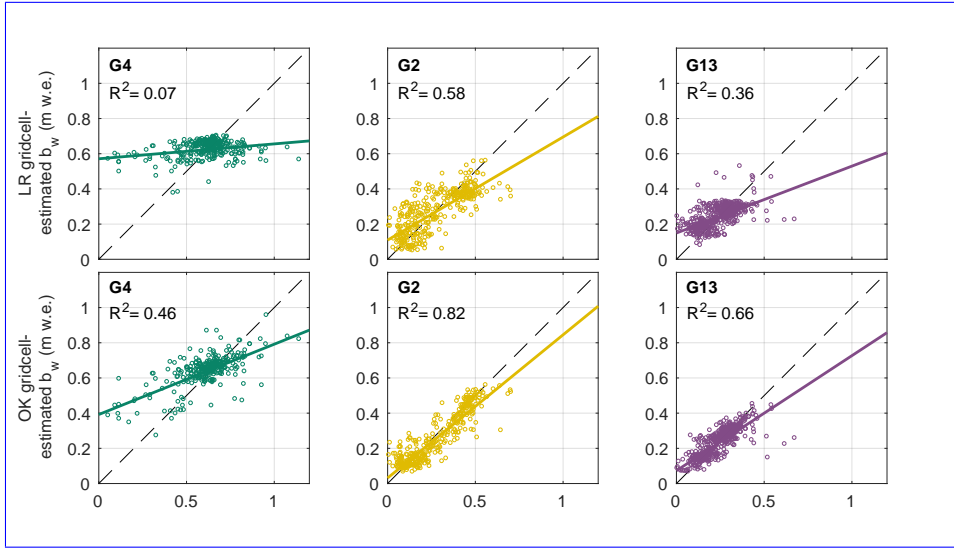451   that interpolation uncertainty contributes more to B_w uncertainty than grid-scale uncertainty or density

Fig. 6. Winter balance (b_w) estimated by linear regression (LR, top row) or ordinary kriging (OK, bottom row) versus the grid-cell averaged b_w data for Glacier 4 (left), Glacier 2 (middle) and Glacier 13 (right). Each circle represents a single gridcell. Explained variance (R^2) is provided. Best-fit (solid) and one-to-one (dashed) lines are shown.

452   assignment method. In other words, the distribution of B_w that arises from grid-scale uncertainty and

453   the differences in distributions between methods of density assignment are smaller than the distribution

454   that arises from interpolation uncertainty (Fig. 7 and Table 5). The B_w distributions obtained using LR

455   and OK overlap for a given glacier, but the distribution modes differ (Fig. 7). OK-estimated values of b_w

456   in the accumulation area are generally lower (Fig. 4), which lowers the B_w estimate. The uncertainty in

457   OK-estimated values of B_w is large, and unrealistic B_w values of 0 m w.e. can be estimated (Fig. 7).

458   The values of B_w for our study glaciers (using LR and S2 density assignment method), with an uncertainty

459   equal to one standard deviation of the distribution found with Monte Carlo analysis, are: 0.59 ± 0.03 m w.e.

460   for Glacier 4, 0.61 ± 0.05 m w.e. for Glacier 2 and 0.40 ± 0.03 m w.e. for Glacier 13. The B_w uncertainty from

Table 5. Standard deviation ($\times 10^{-2}$ m w.e.) of glacier-wide winter balance (B_w) distributions arising from uncertainties in grid-scale b_w (σ_GS), density assignment (σ_ρ), interpolation (σ_INT) and all three sources combined (σ_ALL) for linear regression (left columns) and ordinary kriging (right columns)

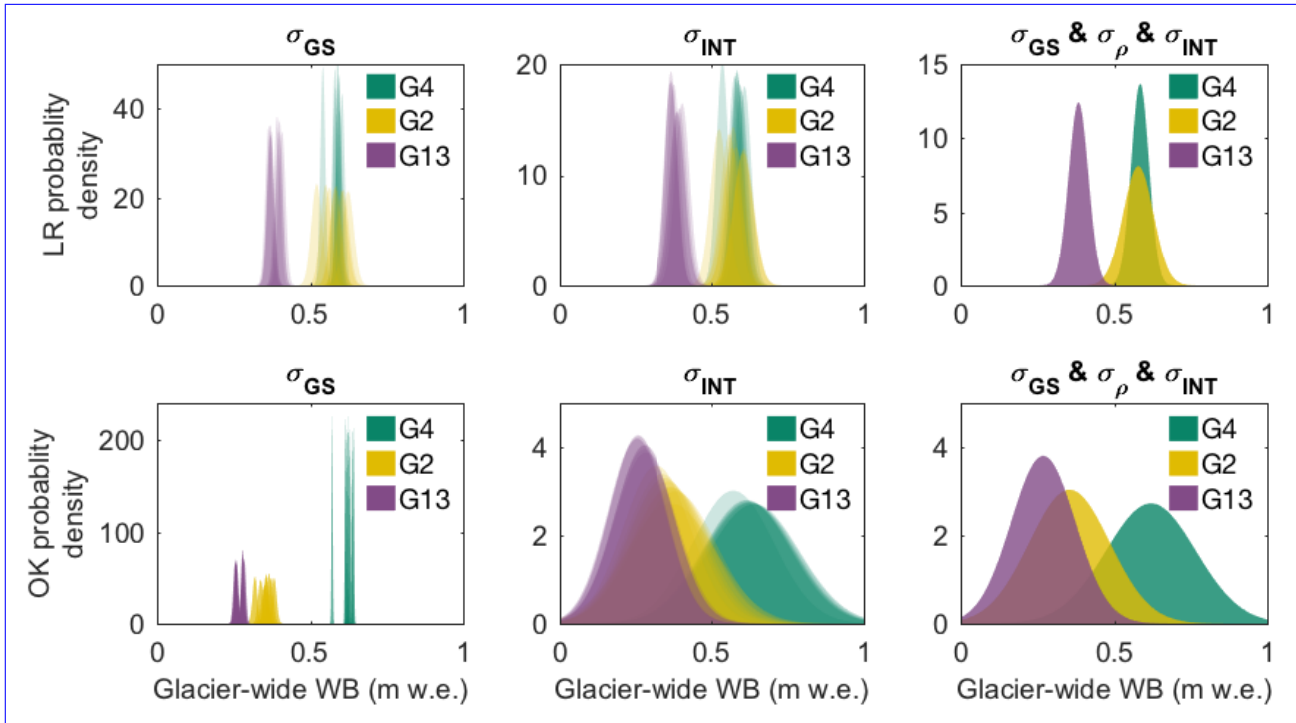|	Linear regression				Ordinary kriging			
	σ_GS	σ_ρ	σ_INT	σ_ALL	σ_GS	σ_ρ	σ_INT	σ_ALL
Glacier 4	0.86	1.90	2.13	2.90	0.18	2.16	14.35	14.64
Glacier 2	1.80	3.37	3.09	4.90	0.80	2.06	12.65	13.14
Glacier 13	1.12	1.68	2.80	3.20	0.57	1.30	9.74	10.48

Fig. 7. ~~Winter~~ Distributions of glacier-wide winter balance (~~WB~~B_w) ~~estimated by linear regression~~ for Glaciers 4 (~~LR~~G4), ~~top row~~2 (G2) ~~or simple kriging~~ and 13 (~~SK, bottom row~~G13) ~~versus the grid-cell-averaged WB data for Glacier 4~~ that arise from various sources of uncertainty. B_w distribution arising from grid-scale uncertainty (σ_{GS}) (left column)~~, Glacier 2~~. B_w distribution arising from interpolation uncertainty (σ_{INT}) (middle column). B_w distribution arising from a combination of σ_{GS}, σ_{INT} and ~~Glacier 13~~ density assignment uncertainty (σ_ρ) (right column). ~~Each circle represents a single gridcell~~Results are shown for interpolation by linear regression (LR, top row) and ordinary kriging (OK, bottom row). ~~Best-fit~~ Left two columns include eight distributions per glacier (~~solid~~colour) and ~~one-to-one~~ each corresponds to a density assignment method (~~dashed~~S1–S4 and F1–F4)~~lines are shown~~.

the three investigated sources of uncertainty ranges from $0.03\,\mathrm{m\,w.e}$ (5%) to $0.05\,\mathrm{m\,w.e}$ (8%) for LR estimates and from $0.10\,\mathrm{m\,w.e}$ (37%) to $0.15\,\mathrm{m\,w.e}$ (24%) for ordinary-kriging estimates (Table 4).

DISCUSSION

Distributed winter balance

Linear regression

Of the topographic parameters in the ~~linear regression~~LR, elevation (z) is the most significant predictor of gridcell-averaged ~~WB~~ b_w for Glaciers 2 and 13, while wind redistribution (Sx) is the most significant predictor for Glacier 4 (Fig. 8~~, Fig. 4~~). As expected, gridcell-averaged ~~WB~~ b_w is positively correlated with elevation where the correlation is significant. It is possible that the elevation correlation was accentuated
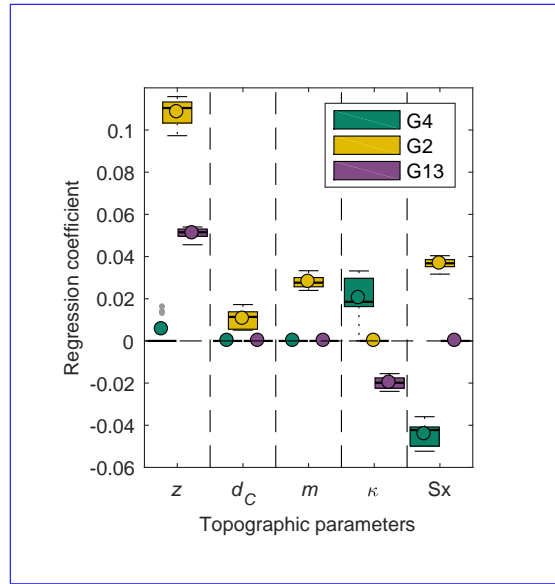
Fig. 8. Distribution of coefficients (β_i) determined by linear regression of gridcell-averaged b_w on DEM-derived topographic parameters for the eight different density assignment methods (Table 3). Coefficients are calculated using standardized data, so values can be compared across parameters. Regression coefficients that are not significant are assigned a value of zero. Topographic parameters include elevation (z), distance from centreline (d_C), slope (m), curvature (κ) and wind redistribution (Sx). Aspect (α) and "northness" (N) are not shown because coefficient values are zero in every case. The box plot shows first quartiles (box), median (line within box), mean (circle within box), minimum and maximum values excluding outliers (bars) and outliers (gray dots), which are defined as being outside of the range of 1.5 times the quartiles (approximately $\pm 2.7\sigma$).

due to melt onset for Glacier 13 in particular. ~~Many studies~~ Glacier 2 had little snow at the terminus likely due to steep slopes and wind-scouring but the snow did not appear to have been affected by melt. Our results are consistent with many studies that have found elevation to be the most significant predictor of ~~winter-balance data (e.g. Machguth and others, 2006; McGrath and others, 2015). However, WB–elevation gradients vary considerably between glaciers (e.g. Winther and others, 1998) and other factors, such as glacier shape and orientation relative to dominant wind direction, are strong predictors of the winter-balance distribution (Machguth and others, 2006; Grabiec and others, 2011). Some studies find no significant correlation between WB on glaciers and topographic parameters, with~~ seasonal snow accumulation data (e.g. Machguth and others, 2006; Grünewald and others, 2014; McGrath and others, 2015). The b_w–elevation gradient is $13\,\mathrm{mm}\,100\,\mathrm{m}^{-1}$ on Glacier 2 and $7\,\mathrm{mm}\,100\,\mathrm{m}^{-1}$ on Glacier 13. These gradients are consistent with those reported for a few glaciers in Svalbard (Winther and others, 1998) but are considerably smaller than many reported b_w–elevation gradients, which range from about 60 to $240\,\mathrm{mm}\,100\,\mathrm{m}^{-1}$

482   (e.g. Hagen and Liestøl, 1990; Tveit and Killingtveit, 1994; Winther and others, 1998). Extrapolating linear

483   relationships to unmeasured locations typically results in considerable estimation error, as seen by the large

484   b_w values (Fig. 4) and large relative uncertainty (Fig. 5) in the high-elevation regions of Glaciers 2 and 13.

485   The low correlation between b_w and elevation on Glacier 4 is consistent with Grabiec and others (2011)

486   and López-Moreno and others (2011), who conclude that highly variable distributions of snow ~~can be~~

487   attributed to complex interactions between topography and the atmosphere that ~~could not~~ cannot be easily

488   quantified ~~(e.g. Grabiec and others, 2011; López-Moreno and others, 2011). Extrapolating relationships to~~

489   ~~unmeasured locations, especially the accumulation area, is susceptible to large uncertainties (Fig. 5). This~~

490   ~~extrapolation has a considerable effect on values of glacier-wide WB, as the highest values of WB are~~

491   ~~typically found in the accumulation area (Fig. 4).~~. The snow on Glacier 4 also did not appear to have

492   been affected by melt and it is hypothesized that significant wind-redistribution processes, that were not

493   captured by the Sx parameter, covered ice-topography and produced a relatively uniform snow depth across

494   the glacier.

495   Gridcell-averaged ~~WB~~ b_w is negatively correlated with Sx on Glacier 4, counter-intuitively indicating

496   less snow in what would be interpreted as sheltered areas. Gridcell-averaged ~~WB~~ b_w is positively

497   correlated with Sx on Glaciers 2 and 13. ~~Similarly, gridcell-averaged WB is positively correlated with~~

498   ~~curvature on Glacier 4 and negatively correlated on Glaciers 2 and 13. Wind redistribution and~~

499   ~~preferential deposition of snow are known to have a large influence on snow distribution at sub-basin~~

500   ~~scales (e.g. Dadić and others, 2010; Winstral and others, 2013; Gerber and others, 2017).~~ Our results

501   corroborate those of McGrath and others (2015) in a study of six glaciers in Alaska (DEM resolutions of

502   5 m) where elevation and Sx were the only significant parameters for all glaciers; Sx regression coefficients

503   were smaller than elevation regression coefficients, and in some cases, negative. While our results point to

504   wind having an impact on snow distribution, ~~but~~ the wind redistribution parameter (Sx) may not adequately

505   capture these effects at our study sites. For example, Glacier 4 ~~is located in a curved valley with steep side~~

506   has a curvilinear plan-view profile and is surrounded by steep valley walls, so specifying a single cardinal

507   direction for wind may not be adequate. Further, the scale of deposition may be smaller than the resolution

508   of the Sx parameter estimated from the DEM. ~~Our results corroborate those of McGrath and others (2015)~~

509   ~~in a study of six glaciers in Alaska (DEM resolutions of 5 m) where elevation and Sx were the only significant~~

510   ~~parameters for all glaciers; Sx regression coefficients were smaller than elevation regression coefficients, and~~

511   ~~in some cases, negative. In addition to wind redistribution,~~ Creation of a parametrization for sublimation

from blowing snow, which has been shown to be an important mechanism of mass loss from ridges (e.g. Musselman and others, 2015), may also increase the explanatory power of LR for our study sites.

We find that transfer of LR coefficients between glaciers results in large estimation errors. Regression coefficients from Glacier 4 produce the highest RMSE (0.38 m w.e. on Glacier 2 and 0.40 m w.e. on Glacier 13, see Table 4 for comparison) and B_w values are the same for all glaciers (0.64 m w.e.) due to the dominance of the regression intercept. Even if the LR is performed with b_w values from all glaciers combined, the resulting coefficients produce large RMSE when applied to individual glaciers (0.31 m w.e., 0.15 m w.e. and 0.14 m w.e. for Glaciers 4, 2 and 13, respectively). Our results are consistent with those of Grünewald and others (2013), who found that local statistical models cannot be transferred across basins and that regional-scale models are not able to explain the majority of observed variance in winter balance.

Ordinary kriging

Due to a paucity of data, simple kriging produces almost uniform gridcell-estimated b_w in the accumulation area of each glacier, inconsistent with observations described in the literature (e.g. Machguth and others, 2006; Grabiec and others, 2011). Glacier 4 has the highest estimated mean with large deviations from the mean at measurement locations. The longer correlation lengths of the data for Glaciers 2 and 13 result in a more smoothly varying distributed b_w. As expected, extrapolation using OK leads to large uncertainty (Fig. 5), further emphasizing the need for spatially distributed point-scale measurements.

LR and OK comparison

LR and OK produce similar estimates of distributed b_w (Fig. 5) and B_w (~0.60 m w.e., Table 4) for Glacier 4 but both are relatively poor

predictors of ~~WB~~ b_w in measured gridcells (~~Table 4~~Fig. 6). For Glaciers 2 and 13, ~~SK~~ OK estimates are more than ~~0.1~~$\sim$0.22 m w.e. (~~up to 40%)~~39%) and $\sim$0.11 m w.e. (30%) lower than LR estimates, respectively (Table 4). RMSE as a percentage of the B_w is lower for OK than LR only for Glacier 4 but the absolute RMSE of OK is $\sim$0.03 m w.e. lower for all glaciers, likely because OK is a data-fitting interpolation method (Table 4). RMSE as a percentage of the glacier-wide WB are comparable between LR and ~~SK~~ OK (Table 4) with an average RMSE of 22%. This comparability is interesting, given that all of the data were used to generate the ~~SK~~ OK model, while only 2/3 were used in the LR. Tests in which only 2/3 of the data were used in the OK model yielded similar results to those in which all data were used. Gridcell-estimated values of ~~WB~~ b_w found using LR and ~~SK~~ OK differ markedly in the upper accumulation areas of Glaciers 2 and 13~~(Fig. 4)~~, where observations are sparse and topographic parameters, such as elevation, vary considerably. The influence of elevation results in substantially higher LR-estimated values of ~~WB~~ b_w at high elevation, whereas ~~SK-estimated values approximate the nearest data~~OK-estimated values are more uniform. Estimates of ablation-area-wide ~~WB~~ B_w differ by <~~7~~6% between LR and ~~SK~~ OK on each glacier, further emphasizing the combined ~~role~~ influence of interpolation method and measurement scarcity in the accumulation area on ~~glacier-wide WB~~ B_w estimates.

~~Distributions of glacier-wide winter balance (WB) for Glaciers 4 (G4), 2 (G2) and 13 (G13) that arise from various sources of uncertainty. WB distribution arising from grid-scale uncertainty (σ_{GS}) (left column). WB distribution arising from interpolation uncertainty (σ_{INT}) (middle column). WB distribution arising from a combination of σ_{GS}, σ_{INT} and density assignment uncertainty (σ_ρ) (right column). Results are shown for interpolation by linear regression (LR, top row) and simple kriging (SK, bottom row). Left two columns include eight distributions per glacier (colour) and each corresponds to a density assignment method (S1–S4 and F1–F4).~~

Uncertainty analysis using a Monte Carlo approach

~~Uncertainty analysis~~

~~Glacier-wide winter balance is affected by uncertainty introduced by the representativeness of gridcell-averaged values of WB (σ_{GS}), choosing a method of density assignment (σ_ρ), and interpolating WB values across the domain (σ_{INT}). Using a Monte Carlo analysis, we find that interpolation uncertainty contributes more to WB uncertainty than grid-scale uncertainty or density assignment method. In other words, the distribution of glacier-wide WB that arises from grid-scale uncertainty and the differences in distributions between methods of density assignment are smaller than the distribution that arises from~~

572 ~~interpolation uncertainty (Fig. 7 and Table 5). The WB distributions obtained using LR and SK overlap~~
573 ~~for a given glacier, but the distribution modes differ (Fig. 7). For reasons outlined above, SK-estimated~~
574 ~~values of WB in the accumulation area are generally lower, which lowers the glacier-wide WB estimate. The~~
575 ~~uncertainty in SK-estimated values of WB is large, and unrealistic glacier-wide values of WB of 0 m w.e. can~~
576 ~~be estimated (Fig. 7). Our~~ Interpolation/extrapolation of b_w data is the largest contributor of B_w uncertainty
577 in our study. These results caution strongly against including ~~extrapolated values of WB~~ values of B_w in
578 comparisons with remote sensing- or model-derived estimates of ~~WB~~B_w. If possible, such comparisons should
579 be restricted to point-scale data.

580 ~~Standard deviation ($\times 10^{-2}$ m w.e.) of glacier-wide winter balance distributions arising from uncertainties~~
581 ~~in grid-scale WB (σ_{GS}), density assignment (σ_ρ), interpolation (σ_{INT}) and all three sources combined (σ_{ALL})~~
582 ~~for linear regression (left columns) and simple kriging (right columns) σ_{GS} σ_ρ σ_{INT} σ_{ALL} σ_{GS} σ_ρ σ_{INT} σ_{ALL}~~
583 ~~**Glacier 4** 0.86 1.90 2.13 2.90 0.85 2.15 14.05 14.72 **Glacier 2** 1.80 3.37 3.09 4.90 2.53 2.03 13.78 13.44~~
584 ~~**Glacier 13** 1.12 1.68 2.80 3.20 1.15 1.27 9.65 10.43~~

585 Grid-scale uncertainty (σ_{GS}) is the smallest assessed contributor to overall ~~WB~~ B_w uncertainty. This result
586 is consistent with the generally smoothly-varying snow depths encountered in zigzag surveys, and previously
587 reported ice-roughness lengths on the order of centimetres (e.g. Hock, 2005) compared to snow depths on the
588 order of decimetres to metres. Given our assumption that zigzags are an adequate representation of grid-scale
589 variability, the low ~~WB~~ B_w uncertainty arising from σ_{GS} implies that subgrid-scale sampling need not be a
590 high priority for reducing overall uncertainty. Our assumption that the 3–4 zigzag surveys can be used to
591 estimate glacier-wide σ_{GS} may be flawed, particularly in areas with debris cover, crevasses and steep slopes.
592 Our analysis did not include uncertainty arising from ~~a number of sources, which we assume either to~~
593 ~~be encompassed by the sources investigated or to be negligible contributors. These sources of uncertainty~~
594 ~~include~~ density measurement errors associated with the ~~Federal Sampler~~FS, wedge cutters and spring scales,
595 from vertical and horizontal errors in the DEM ~~and~~ or from error associated with estimating measurement
596 locations ~~.~~
597 ~~The values of glacier-wide WB for our study glaciers (using LR and S2 density assignment method), with~~
598 ~~an uncertainty equal to one standard deviation of the distribution found with Monte Carlo analysis, are:~~
599 ~~0.59 ± 0.03 m w. e. for Glacier 4, 0.61 ± 0.05 m w.e. for Glacier 2 and 0.40 ± 0.03 m w.e. for Glacier 13. The~~
600 ~~glacier-wide WB uncertainty from combined~~ based on the GPS position of the lead observer. We assume that
601 these sources of uncertainty ~~ranges from 0.03 m w. e (5%) to 0.05 m w.e (8%) for linear-regression estimates~~

and from 0.10 m w.e (37%) to 0.15 m w.e (24%) for simple-kriging estimates (Table 4). are either encompassed by the sources investigated or are negligible.

~~Context and caveats~~Regional winter-balance gradient

~~Regional winter-balance gradient~~

Although we find considerable inter- and intra-basin variability in winter balance, our results are consistent with a regional-scale winter-balance gradient for the continental side of the St. Elias Mountains (Fig. 9). Winter-balance data are compiled from Taylor-Barge (1969), the three glaciers presented in this paper and two ~~snow pits~~ SP we analyzed near the head of the Kaskawulsh Glacier between 20–21 May 2016. The data show a linear decrease of $0.024 \, \mathrm{m \, w.e. \, km^{-1}}$ ($R^2 = 0.85$) in winter balance with distance from the regional topographic divide between the Kaskawulsh and Hubbard Glaciers, as identified by Taylor-Barge (1969). While the three study glaciers fit the regional trend, the same relationship would not apply if just the Donjek Range were considered. We hypothesize that interaction between meso-scale weather patterns and large-scale mountain topography is a major driver of regional-scale winter balance. Further insight into regional-scale patterns of winter balance in the St. Elias Mountains could be gained by investigating moisture source trajectories and the contribution of orographic precipitation.

~~Limitations and future work~~

Limitations and future work

The potential limitations of our work include the restriction of our data to a single year, minimal sampling in the accumulation area, the problem of uncorrelated SP- and FS-derived densities, a sampling design that could not be optimized ~~a priori~~*a priori*, the assumption of spatially uniform subgrid variability and lack of more finely resolved DEMs.

Inter-annual variability in winter balance is not considered in our study. A number of studies have found temporal stability in spatial patterns of snow distribution and that statistical models based on topographic parameters could be applied reliably between years (e.g. Grünewald and others, 2013). For example, Walmsley (2015) analyzed more than 40 years of winter balance recorded on two Norwegian glaciers and found that snow distribution is spatially heterogeneous yet exhibits robust temporal stability. Contrary to this, Crochet and others (2007) found that snow distribution in Iceland differed considerably between years and depended primarily on the dominant wind direction over the course of a winter. Therefore, multiple years of snow depth
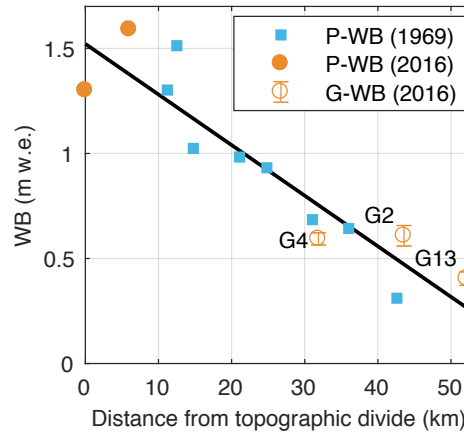
Fig. 9. Relationship between winter balance ~~(WB)~~ and linear distance from the regional topographic divide between the Kaskawulsh and Hubbard Glaciers in the St. Elias Mountains. Point-scale values of ~~WB~~ winter balance from snow-pit data reported by Taylor-Barge (1969) (blue boxes, P-WB). LR-estimated glacier-wide ~~WB~~ winter balance (B_{w}) calculated using density assignment S2 for Glaciers 4 (G4), 2 (G2) and 13 (G13) with errors bars calculated as the standard deviation of Monte Carlo-derived ~~WB~~ B_{w} distributions (this study) (open orange circles, G-WB). Point-scale ~~WB~~ winter balance estimated from snow-pit data at two locations in the accumulation area of the Kaskawulsh Glacier, collected in May 2016 (unpublished data, SFU Glaciology Group) (filled orange dots, P-WB). Black line indicates best fit ($R^2 = 0.85$).

630 and density measurements, that are not necessarily consecutive, are needed to better understand inter-annual

631 variability ~~in winter-balance distribution~~ of winter balance within the Donjek Range.

632   There is a conspicuous lack of data in the accumulation areas of our study glaciers. With increased sampling

633 in the accumulation area, interpolation uncertainties would be reduced where they are currently greatest

634 and the ~~linear regression~~ LR would be better constrained. Although certain regions of the glaciers remain

635 inaccessible for direct measurements, other methods of obtaining winter-balance measurements, including

636 ground-penetrating radar and DEM differencing with photogrammetry or lidar, could be used in conjunction

637 with manual probing to increase the spatial coverage of measurements.

638   The lack of correlation between SP- and FS-derived densities needs to be reconciled. Contrary to our

639 results, most studies that compare SP- and FS-derived densities report minimal discrepancy (e.g. Dixon

640 and Boon, 2012, and sources within). Additional co-located density measurements are needed to better

641 compare the two methods of obtaining density values. Comparison with other ~~Federal Samplers~~ FS would

642 also be informative. Even with this limitation, density assignment was, fortunately, not the largest source of

643 uncertainty in estimating glacier-wide winter balance.

Our sampling design was chosen to achieve broad spatial coverage of the ablation area, but is likely too finely resolved along transects for many mass-balance surveys to replicate. An optimal sampling design would minimize uncertainty in winter balance while reducing the number of required measurements. Analysis of the estimated winter balance obtained using subsets of the data is underway to make recommendations on optimal transect configuration and along-track spacing of measurements. López-Moreno and others (2010) found that 200–400 observations are needed within a non-glacierized alpine basin ($6\,\mathrm{km}^2$) to obtain accurate and robust snow distribution models. Similar guidelines would be useful for glacierized environments.

In this study, we assume that the subgrid variability of winter balance is uniform across a given glacier. Contrary to this assumption, McGrath and others (2015) found greater variability of winter-balance values close to the terminus. Testing our assumption could be a simple matter of prioritizing the labour-intensive zigzags surveys. To ensure consistent quantification of subgrid variability, zigzag survey measurements could also be tested against other measurements methods, such as lidar.

DEM gridcell size is known to influence values of computed topographic parameters (Zhang and Montgomery, 1994; Garbrecht and Martz, 1994; Guo-an and others, 2001; López-Moreno and others, 2010). The relationship between topographic parameters and winter balance is, therefore, not independent of DEM gridcell size. For example, Kienzle (2004) and López-Moreno and others (2010) found that a decrease in spatial resolution of the DEM results in a decrease in the importance of curvature and an increase in the importance of elevation in ~~regressions~~ LR of snow distribution on topographic parameters in non-glacierized basins. The importance of curvature in our study is affected by the DEM smoothing that we applied to obtain a spatially continuous curvature field (see Supplementary Material, Fig. S1). A comparison of regression coefficients from high-resolution DEMs obtained from various sources and sampled with various gridcell sizes could be used to characterize the dependence of topographic parameters on DEMs, and therefore assess the robustness of inferred relationships between winter balance and topographic parameters.

CONCLUSION

We estimate winter balance for three glaciers (termed Glacier 2, Glacier 4 and Glacier 13) in the St. Elias Mountains, Yukon, Canada from multiscale snow depth and density measurements. Linear regression and ~~simple~~ ordinary kriging are used to obtain estimates of distributed winter balance (b_w). We use Monte Carlo analysis to evaluate the contributions of interpolation, ~~the~~ assignment of snow density and grid-scale variability of winter balance to uncertainty in estimates of glacier-wide winter balance (B_w).

Values of ~~glacier-wide winter balance~~ B_w estimated using linear regression and ~~simple~~ ordinary kriging differ by up to 0.24 m w.e. (∼50%). We find that interpolation uncertainty is the largest assessed source of uncertainty in ~~glacier-wide winter balance (5~~B_w (7% for linear-regression estimates and ~~32% for simple-kriging~~ 34% for ordinary-kriging estimates). Uncertainty resulting from the method of density assignment is comparatively low, despite the wide range of methods explored. Given our representation of grid-scale variability, the resulting ~~winter balance~~ B_w uncertainty is small indicating that extensive subgrid-scale sampling is not required to reduce overall uncertainty.

Our results suggest that processes governing distributed ~~winter balance~~ b_w differ between glaciers, highlighting the importance of regional-scale winter-balance studies. The estimated distribution of ~~winter balance~~ b_w on Glacier 4 is characterized by high variability, as indicated by the poor correlation between estimated and observed values and large number of data outliers. Glaciers 2 and 13 appear to have lower spatial variability, with elevation being the dominant predictor of gridcell-averaged ~~winter balance~~b_w. A wind-redistribution parameter is found to be a weak but significant predictor of ~~winter balance~~b_w, though conflicting relationships between glaciers make it difficult to interpret. The major limitations of our work include the restriction of our data to a single year and minimal sampling in the accumulation area. Although challenges persist when estimating winter balance, our data are consistent with a regional-scale winter-balance gradient for the continental side of the St. Elias Mountains.

AUTHOR CONTRIBUTION STATEMENT

AP planned and executed the data collection, performed all calculations and drafted the manuscript. GF conceived of the study, contributed to field planning and data collection, oversaw all stages of the work and edited the manuscript. VR provided guidance with statistical methods and edited the manuscript.

ACKNOWLEDGEMENTS

702 5 DEM and for assistance in DEM correction. We are grateful to Derek Bingham and Michael Grosskopf

703 for assistance with the statistics, including ~~simple~~ ordinary kriging. Luke Wonneck, Leif Anderson and Jeff

704 Crompton all provided thoughtful and constructive comments on drafts of the manuscript.

REFERENCES

706 Anderton S, White S and Alvera B (2004) Evaluation of spatial variability in snow water equivalent for a high

707   mountain catchment. *Hydrological Processes*, **18**(3), 435–453 (doi: 10.1002/hyp.1319)

708 Arendt AA, Luthcke SB, Larsen CF, Abdalati W, Krabill WB and Beedle MJ (2008) Validation of high-resolution

709   GRACE mascon estimates of glacier mass changes in the St Elias Mountains, Alaska, USA, using aircraft laser

710   altimetry. *Journal of Glaciology*, **54**(188), 778–787 (doi: 10.3189/002214308787780067)

711 Bagos PG and Adam M (2015) On the Covariance of Regression Coefficients. *Open Journal of Statistics*, **5**, 680–701

712   (doi: 10.4236/ojs.2015.57069)

713 Balk B and Elder K (2000) Combining binary decision tree and geostatistical methods to estimate snow distribution

714   in a mountain watershed. *Water Resources Research*, **36**(1), 13–26 (doi: 10.1029/1999WR900251)

715 Barry RG (1992) *Mountain weather and climate.* Cambridge Univserity Press, 3rd edition

716 Beaumont RT and Work RA (1963) Snow sampling results from three samplers. *International Association of Scientific

717   Hydrology. Bulletin*, **8**(4), 74–78 (doi: 10.1080/02626666309493359)

718 Burgess EW, Forster RR and Larsen CF (2013) Flow velocities of Alaskan glaciers. *Nature communications*, **4**,

719   2146–2154 (doi: 10.1038/ncomms3146)

720 Burnham KP and Anderson DR (2004) Multimodel Inference: Understanding AIC and BIC in Model Selection.

721   *Sociological Methods & Research*, **33**(2), 261–304 (doi: 10.1177/0049124104268644)

722 Carroll T (1977) A comparison of the CRREL $500\,cm^3$ tube and the ILTS 200 and $100\,cm^3$ box cutters used for

723   determining snow densities. *Journal of Glaciology*, **18**(79), 334–337 (doi: 10.1017/S0022143000021420)

724 Clark MP, Hendrikx J, Slater AG, Kavetski D, Anderson B, Cullen NJ, Kerr T, Örn Hreinsson E and Woods RA

725   (2011) Representing spatial variability of snow water equivalent in hydrologic and land-surface models: A review.

726   *Water Resources Research*, **47**(7) (doi: 10.1029/2011WR010745)

727 Clarke GK (2014) A short and somewhat personal history of Yukon glacier studies in the Twentieth Century. *Arctic*,

728   **37**(1), 1–21

729 Clyde GD (1932) Circular No. 99-Utah Snow Sampler and Scales for Measuring Water Content of Snow. *UAES

730   Circulars*, Paper 90

731 Cogley J, Hock R, Rasmussen L, Arendt A, Bauder A, Braithwaite R, Jansson P, Kaser G, Möller M, Nicholson L

732   and others (2011) *Glossary of glacier mass balance and related terms.* UNESCO-IHP, Paris

Conger SM and McClung DM (2009) Comparison of density cutters for snow profile observations. *Journal of Glaciology*, **55**(189), 163–169 (doi: 10.3189/002214309788609038)

Crochet P, Jóhannesson T, Jónsson T, SigurÃřsson O, Björnsson H, Pálsson F and Barstad I (2007) Estimating the Spatial Distribution of Precipitation in Iceland Using a Linear Model of Orographic Precipitation. *Journal of Hydrometeorology*, **8**(6), 1285–1306 (doi: 10.1175/2007JHM795.1)

Crompton JW and Flowers GE (2016) Correlations of suspended sediment size with bedrock lithology and glacier dynamics. *Annals of Glaciology*, **57**(72), 1–9 (doi: 10.1017/aog.2016.6)

Cullen NJ, Anderson B, Sirguey P, Stumm D, Mackintosh A, Conway JP, Horgan HJ, Dadic R, Fitzsimons SJ and Lorrey A (2017) An 11-year record of mass balance of Brewster Glacier, New Zealand, determined using a geostatistical approach. *Journal of Glaciology*, **63**(238), 199–217 (doi: 10.1017/jog.2016.128)

Dadić R, Mott R, Lehning M and Burlando P (2010) Parameterization for wind-induced preferential deposition of snow. *Journal of Geophysical Research: Earth Surface*, **24**(14), 1994–2006 (doi: 10.1029/2009JF001261)

Danby RK, Hik DS, Slocombe DS and Williams A (2003) Science and the St. Elias: an evolving framework for sustainability in North America's highest mountains. *The Geographical Journal*, **169**(3), 191–204 (doi: 10.1111/1475-4959.00084)

Davis JC and Sampson RJ (1986) *Statistics and data analysis in geology*. Wiley New York et al., 2nd edition

Deems JS and Painter TH (2006) Lidar measurement of snow depth: accuracy and error sources. In *Proceedings of the International Snow Science Workshop*

Dixon D and Boon S (2012) Comparison of the SnowHydro snow sampler with existing snow tube designs. *Hydrological Processes*, **26**(17), 2555–2562 (doi: 10.1002/hyp.9317)

Egli L, Griessinger N and Jonas T (2011) Seasonal development of spatial snow-depth variability across different scales in the Swiss Alps. *Annals of Glaciology*, **52**(58), 216–222 (doi: 10.3189/172756411797252211)

Elder K, Dozier J and Michaelsen J (1991) Snow accumulation and distribution in an alpine watershed. *Water Resources Research*, **27**(7), 1541–1552 (doi: 10.1029/91WR00506)

Elder K, Rosenthal W and Davis RE (1998) Estimating the spatial distribution of snow water equivalence in a montane watershed. *Hydrological Processes*, **12**(1011), 1793–1808 (doi: 10.1002/(SICI)1099-1085(199808/09)12:10/111793::AID-HYP6953.0.CO;2-K)

Erxleben J, Elder K and Davis R (2002) Comparison of spatial interpolation methods for estimating snow distribution in the Colorado Rocky Mountains. *Hydrological Processes*, **16**(18), 3627–3649 (doi: 10.1002/hyp.1239)

Fames PE, Peterson N, Goodison B and Richards RP (1982) Metrication of Manual Snow Sampling Equipment. In *Proceedings of the 50th Western Snow Conference*, 120–132

764 Fierz C, Armstrong RL, Durand Y, Etchevers P, Greene E, McClung DM, Nishimura K, Satyawali PK and Sokratov

765   SA (2009) *The international classification for seasonal snow on the ground.* UNESCO/IHP, unesco/ihp paris

766   edition

767 Garbrecht J and Martz L (1994) Grid size dependency of parameters extracted from digital elevation models.

768   *Computers & Geosciences*, **20**(1), 85–87 (doi: 10.1016/0098-3004(94)90098-1)

769 Gerber F, Lehning M, Hoch SW and Mott R (2017) A close-ridge small-scale atmospheric flow field and its

770   influence on snow accumulation. *Journal of Geophysical Research: Atmospheres*, **122**(15), 7737–7754 (doi:

771   10.1002/2016JD026258), 2016JD026258

772 Grabiec M, Puczko D, Budzik T and Gajek G (2011) Snow distribution patterns on Svalbard glaciers derived from

773   radio-echo soundings. *Polish Polar Research*, **32**(4), 393–421 (doi: 10.2478/v10183-011-0026-4)

774 Gray DM and Male DH (1981) *Handbook of snow: principles, processes, management & use.* Pergamon Press, 1st

775   edition

776 Grünewald T, Schirmer M, Mott R and Lehning M (2010) Spatial and temporal variability of snow depth and ablation

777   rates in a small mountain catchment. *Cryosphere*, **4**(2), 215–225 (doi: 10.5194/tc-4-215-2010)

778 Grünewald T, Stötter J, Pomeroy J, Dadic R, Moreno Baños I, Marturià J, Spross M, Hopkinson C, Burlando P

779   and Lehning M (2013) Statistical modelling of the snow depth distribution in open alpine terrain. *Hydrology and*

780   *Earth System Sciences*, **17**(8), 3005–3021 (doi: 10.5194/hess-17-3005-2013)

781 Grünewald T, Bühler Y and Lehning M (2014) Elevation dependency of mountain snow depth. *The Cryosphere*, **8**(6),

782   2381–2394 (doi: 10.5194/tc-8-2381-2014)

783 Guo-an T, Yang-he H, Strobl J and Wang-qing L (2001) The impact of resolution on the accuracy of hydrologic data

784   derived from DEMs. *Journal of Geographical Sciences*, **11**(4), 393–401 (doi: 10.1007/BF02837966)

785 Gusmeroli A, Wolken GJ and Arendt AA (2014) Helicopter-borne radar imaging of snow cover on and around glaciers

786   in Alaska. *Annals of Glaciology*, **55**(67), 78–88 (doi: 10.3189/2014AoG67A029)

787 Hagen JO and Liestøl O (1990) Long-term glacier mass-balance investigations in Svalbard, 1950-88. *Annals of*

788   *Glaciology*, **14**(1), 102–106

789 Helbig N and van Herwijnen A (2017) Subgrid parameterization for snow depth over mountainous terrain from flat

790   field snow depth. *Water Resources Research*, **53**(2), 1444–1456 (doi: 10.1002/2016WR019872)

791 Hock R (2005) Glacier melt: a review of processes and their modelling. *Progress in Physical Geography*, **29**(3), 362–391

792   (doi: 10.1191/0309133305pp453ra)

793 Hock R and Jensen H (1999) Application of kriging interpolation for glacier mass balance computations. *Geografiska*

794   *Annaler: Series A, Physical Geography*, **81**(4), 611–619 (doi: 10.1111/1468-0459.00089)

795 Kaser G, Fountain A, Jansson P and others (2003) *A manual for monitoring the mass balance of mountain glaciers.*

796   ICSI/UNESCO

Kienzle S (2004) The Effect of DEM Raster Resolution on First Order, Second Order and Compound Terrain Derivatives. *Transactions in GIS*, **8**(1), 83–111 (doi: 10.1111/j.1467-9671.2004.00169.x)

Kinar N and Pomeroy J (2015) Measurement of the physical properties of the snowpack. *Reviews of Geophysics*, **53**(2), 481–544 (doi: 10.1002/2015RG000481)

Kohavi R and others (1995) A study of cross-validation and bootstrap for accuracy estimation and model selection. In *Proceedings of the Fourteenth International Joint Conference on Artificial Intelligence*, 1137–1145

Korona J, Berthier E, Bernard M, Rémy F and Thouvenot E (2009) SPIRIT SPOT 5 stereoscopic survey of Polar Ice: Reference images and topographies during the fourth International Polar Year (2007–2009). *ISPRS Journal of Photogrammetry and Remote Sensing*, **64**(2), 204–212 (doi: 10.1016/j.isprsjprs.2008.10.005)

Lehning M, Völksch I, Gustafsson D, Nguyen TA, Stähli M and Zappa M (2006) ALPINE3D: a detailed model of mountain surface processes and its application to snow hydrology. *Hydrological Processes*, **20**(10), 2111–2128 (doi: 10.1002/hyp.6204)

Li J and Heap AD (2008) A review of spatial interpolation methods for environmental scientists. *Geoscience Australia*, Record 2008/23

Liston GE and Elder K (2006) A distributed snow-evolution modeling system (SnowModel). *Journal of Hydrometeorology*, **7**(6), 1259–1276 (doi: 10.1175/JHM548.1)

Liston GE and Sturm M (1998) A snow-transport model for complex terrain. *Journal of Glaciology*, **44**(148), 498–516

López-Moreno J, Latron J and Lehmann A (2010) Effects of sample and grid size on the accuracy and stability of regression-based snow interpolation methods. *Hydrological Processes*, **24**(14), 1914–1928 (doi: 10.1002/hyp.7564)

López-Moreno J, Fassnacht S, Heath J, Musselman K, Revuelto J, Latron J, Morán-Tejeda E and Jonas T (2013) Small scale spatial variability of snow density and depth over complex alpine terrain: Implications for estimating snow water equivalent. *Advances in Water Resources*, **55**, 40–52 (doi: 10.1016/j.advwatres.2012.08.010)

López-Moreno JI, Fassnacht S, Beguería S and Latron J (2011) Variability of snow depth at the plot scale: implications for mean depth estimation and sampling strategies. *The Cryosphere*, **5**(3), 617–629 (doi: 10.5194/tc-5-617-2011)

MacDougall AH and Flowers GE (2011) Spatial and temporal transferability of a distributed energy-balance glacier melt model. *Journal of Climate*, **24**(5), 1480–1498 (doi: 10.1175/2010JCLI3821.1)

Machguth H, Eisen O, Paul F and Hoelzle M (2006) Strong spatial variability of snow accumulation observed with helicopter-borne GPR on two adjacent alpine glaciers. *Geophysical Research Letters*, **33**(13), 1–5 (doi: 10.1029/2006GL026576)

Madigan D and Raftery AE (1994) Model Selection and Accounting for Model Uncertainty in Graphical Models Using Occam's Window. *Journal of the American Statistical Association*, **89**(428), 1535–1546

828 Marshall HP, Koh G, Sturm M, Johnson J, Demuth M, Landry C, Deems J and Gleason J (2006) Spatial variability of
829   the snowpack: Experiences with measurements at a wide range of length scales with several different high precision
830   instruments. In *Proceedings International Snow Science Workshop*, 359–364

831 McGrath D, Sass L, O'Neel S, Arendt A, Wolken G, Gusmeroli A, Kienholz C and McNeil C (2015) End-of-winter
832   snow depth variability on glaciers in Alaska. *Journal of Geophysical Research: Earth Surface*, **120**(8), 1530–1550
833   (doi: 10.1002/2015JF003539)

834 Metropolis N and Ulam S (1949) The Monte Carlo Method. *Journal of the American Statistical Association*, **44**(247),
835   335–341

836 Molotch N, Colee M, Bales R and Dozier J (2005) Estimating the spatial distribution of snow water equivalent in
837   an alpine basin using binary regression tree models: the impact of digital elevation data and independent variable
838   selection. *Hydrological Processes*, **19**(7), 1459–1479 (doi: 10.1002/hyp.5586)

839 Mott R, Faure F, Lehning M, Löwe H, Hynek B, Michlmayer G, Prokop A and Schöner W (2008) Simulation of
840   seasonal snow-cover distribution for glacierized sites on Sonnblick, Austria, with the Alpine3D model. *Annals of
841   Glaciology*, **49**(1), 155–160 (doi: 10.3189/172756408787814924)

842 Musselman KN, Pomeroy JW, Essery RL and Leroux N (2015) Impact of windflow calculations on simulations
843   of alpine snow accumulation, redistribution and ablation. *Hydrological Processes*, **29**(18), 3983–3999 (doi:
844   10.1002/hyp.10595)

845 Proksch M, Rutter N, Fierz C and Schneebeli M (2016) Intercomparison of snow density measurements: bias, precision,
846   and vertical resolution. *The Cryosphere*, **10**(1), 371–384 (doi: 10.5194/tc-10-371-2016)

847 Pulwicki A (2017) *Multi-scale investigation of winter balance on alpine glaciers*. Master's thesis, Simon Fraser
848   University

849 Raftery AE, Madigan D and Hoeting JA (1997) Bayesian Model Averaging for Linear Regression Models. *Journal of
850   the American Statistical Association*, **92**(437), 179–191 (doi: 10.1080/01621459.1997.10473615)

851 Rasmussen CE and Williams CK (2006) *Gaussian processes for machine learning*. MIT press Cambridge

852 Réveillet M, Vincent C, Six D and Rabatel A (2016) Which empirical model is best suited to simulate glacier mass
853   balances? *Journal of Glaciology*, **63**(237), 1–16 (doi: 10.1017/jog.2016.110)

854 Roustant O, Ginsbourger D and Deville Y (2012) DiceKriging, DiceOptim: Two R packages for the analysis of
855   computer experiments by kriging-based metamodeling and optimization. *Journal of Statistical Software*, **21**, 1–55

856 Schneiderbauer S and Prokop A (2011) The atmospheric snow-transport model: SnowDrift3D. *Journal of Glaciology*,
857   **57**(203), 526–542 (doi: 10.3189/002214311796905677)

858 Schuler TV, Crochet P, Hock R, Jackson M, Barstad I and Jóhannesson T (2008) Distribution of snow accumulation
859   on the Svartisen ice cap, Norway, assessed by a model of orographic precipitation. *Hydrological Processes*, **22**(19),
860   3998–4008 (doi: 10.1002/hyp.7073)

Scipión DE, Mott R, Lehning M, Schneebeli M and Berne A (2013) Seasonal small-scale spatial variability in alpine snowfall and snow accumulation. *Water Resources Research*, **49**(3), 1446–1457, ISSN 1944-7973 (doi: 10.1002/wrcr.20135)

Shea C and Jamieson B (2010) Star: an efficient snow point-sampling method. *Annals of Glaciology*, **51**(54), 64–72 (doi: 10.3189/172756410791386463)

Sold L, Huss M, Hoelzle M, Andereggen H, Joerg PC and Zemp M (2013) Methodological approaches to infer end-of-winter snow distribution on alpine glaciers. *Journal of Glaciology*, **59**(218), 1047–1059 (doi: 10.3189/2013JoG13J015)

Tangborn WV, Krimmel RM and Meier MF (1975) A comparison of glacier mass balance by glaciological, hydrological and mapping methods, South Cascade Glacier, Washington. *International Association of Hydrological Sciences Publication*, **104**, 185–196

Taylor-Barge B (1969) *The summer climate of the St. Elias Mountain region*. Montreal: Arctic Institute of North America, Research Paper No. 53

Thibert E, Blanc R, Vincent C and Eckert N (2008) Glaciological and volumetric mass-balance measurements: error analysis over 51 years for Glacier de Sarennes, French Alps. *Journal of Glaciology*, **54**(186), 522–532

Trujillo E and Lehning M (2015) Theoretical analysis of errors when estimating snow distribution through point measurements. *The Cryosphere*, **9**(3), 1249–1264 (doi: 10.5194/tc-9-1249-2015)

Turcan J and Loijens H (1975) Accuracy of snow survey data and errors in snow sampler measurements. In *32nd Eastern Snow Conference*

Tveit J and Killingtveit Å (1994) Snow surveys for studies of water budget on Svalbard 1991–1994. In *Proceedings of the 10th International Northern Research Basins Symposium and Workshop, Spitsbergen, Norway. SINTEF Report*, volume 22, A96415

Waechter A, Copland L and Herdes E (2015) Modern glacier velocities across the Icefield Ranges, St Elias Mountains, and variability at selected glaciers from 1959 to 2012. *Journal of Glaciology*, **61**(228), 624–634 (doi: 10.3189/2015JoG14J147)

Walmsley APU (2015) *Long-term observations of snow spatial distributions at Hellstugubreen and Gråsubreen, Norway*. Master's thesis, University of Oslo

Wetlaufer K, Hendrikx J and Marshall L (2016) Spatial Heterogeneity of Snow Density and Its Influence on Snow Water Equivalence Estimates in a Large Mountainous Basin. *Hydrology*, **3**(3), 1–17 (doi: 10.3390/hydrology3010003)

Wilson N and Flowers G (2013) Environmental controls on the thermal structure of alpine glaciers. *The Cryosphere*, **7**(1), 167–182 (doi: 10.5194/tc-7-167-2013)

Wilson NJ, Flowers GE and Mingo L (2013) Comparison of thermal structure and evolution between neighboring subarctic glaciers. *Journal of Geophysical Research: Earth Surface*, **118**(3), 1443–1459 (doi: 10.1002/jgrf.20096)

894 Winstral A, Elder K and Davis RE (2002) Spatial snow modeling of wind-redistributed snow using terrain-based pa-
895   rameters. *Journal of Hydrometeorology*, **3**(5), 524–538 (doi: 10.1175/1525-7541(2002)0030524:SSMOWR2.0.CO;2)

896 Winstral A, Marks D and Gurney R (2013) Simulating wind-affected snow accumulations at catchment to basin
897   scales. *Advances in Water Resources*, **55**, 64–79 (doi: 10.1016/j.advwatres.2012.08.011)

898 Winther J, Bruland O, Sand K, Killingtveit A and Marechal D (1998) Snow accumulation distribution on Spitsbergen,
899   Svalbard, in 1997. *Polar Research*, **17**, 155–164 (doi: 10.3402/polar.v17i2.6616)

900 Woo MK and Marsh P (1978) Analysis of Error in the Determination of Snow Storage for Small High Arctic Basins.
901   *Journal of Applied Meteorology*, **17**(10), 1537–1541 (doi: 10.1175/1520-0450(1978)0171537:AOEITD2.0.CO;2)

902 Wood WA (1948) Project "Snow Cornice": the establishment of the Seward Glacial research station. *Arctic*, **1**(2),
903   107–112

904 Work R, Stockwell H, Freeman T and Beaumont R (1965) *Accuracy of field snow surveys*. Cold Regions Research &
905   Engineering Laboratory

906 Zhang W and Montgomery DR (1994) Digital elevation model grid size, landscape representation, and hydrologic
907   simulations. *Water Resources Research*, **30**(4), 1019–1028 (doi: 10.1029/93WR03553)